Science Advances
AAAS

advances.sciencemag.org/cgi/content/full/7/21/eabf0360/DC1

Supplementary Materials for

Gas-phase synthesis of benzene via the propargyl radical self-reaction

Long Zhao, Wenchao Lu, Musahid Ahmed*, Marsel V. Zagidullin, Valeriy N. Azyazov, Alexander N. Morozov, Alexander M. Mebel*, Ralf I. Kaiser*

*Corresponding author. Email: mahmed@lbl.gov (M.A.); mebela@fiu.edu (A.M.M.); ralfk@hawaii.edu (R.I.K.)

Published 21 May 2021, *Sci. Adv.* **7**, eabf0360 (2021)
DOI: 10.1126/sciadv.abf0360

This PDF file includes:

1. Formation of benzene and its isomers via the recombination of two propargyl radicals – Experimental Studies

Thus far, there has been no experiment under high temperature conditions that has monitored the kinetics *and* mechanisms of a RSFR reacting with a second hydrocarbon radical of its kind *in situ* with mass growth processes limited to the very first aromatic ring (Table S1). *First*, previous experiments exploited an *ex-situ* analysis of the products via gas chromatography coupled with mass spectrometry (GC-MS). This approach cannot detect unstable species and reactive intermediates, but can identify in the ex-situ mode only closed shell molecules which are thermally stable at room temperature. Therefore, the molecules detected by GC-MS are not necessarily the nascent reaction products of propargyl-propargyl radical reactions. *Second*, *in-situ* identifications of products of the propargyl-radical self-reaction were conducted at propargyl radical concentrations, which were too high to eliminate mass growth processes beyond benzene up to phenanthrene ($C_{14}H_{10}$). These 'dense' environments do not allow the extraction of the reaction mechanisms leading to the formation of the initial aromatic product – benzene – since successive reactions can convert benzene and its isomers to higher molecular mass growth products.

In detail, kinetic studies of the propargyl radical self-reaction determined rate constants in the range from 1×10^{-11} cm^3 s^{-1} to 4×10^{-11} cm^3 s^{-1} covering temperatures between 295 K and 1,500 K and pressures from 2 to 800 Torr (*67-79*) with products characterized *off-line* by gas chromatography coupled with mass spectrometry (GC-MS). These studies revealed the formation of 1,5-hexadiyne (60%), 1,2-hexdiene-5-yne (25%) along with an unidentified C_6H_6 isomer (15%) (*69*) and of 1,5-hexadiyne (27%), fulvene (1%), 3,4-dimethylenecyclobutene (47%), 1,2-hexdiene-5-yne (22%), and benzene (3%) at temperatures reaching 623 K and pressures of 933 mbar (*70*). GC-MS was also exploited to detect 1,5-hexadiyne and benzene as well as 1,5-hexadiyne (1%), 1,2-hexadiene-5-yne, 3,4-dimethylene-cyclobutene, 2-ethynyl-1,3-butadiene, fulvene, benzene, and *cis*-/*trans*-1,3-hexadiene-5-yne in high temperature (1,100–2,100 K (*71*), 720-1,350 K (*77*)) shock tube experiments from 1,100 to 1,700 Torr (*71*) and 18,700 to 37,500 Torr (*77*), respectively. In the latter study, branching ratios of C_6H_6 isomers were extracted to be 1,5-hexadiyne (1%), 1,2-hexadiene-5-yne (12%), 3,4-dimethylene-cyclobutene (45%), 2-ethynyl-1,3-butadiene (13%), fulvene (20%), benzene (2%), and *cis*-

/*trans*-1,3-hexadiene-5-yne (7%) (*77*). Besides the GC-MS detection of 1,5-hexadiyne (1% at 1,100 K), fulvene (7% at 1,100 K), and benzene (87% at 1,100 K), the identification of higher molecular mass growth products phenylacetylene (C_6H_5CCH) and indene (C_9H_8) was attributed to reactions of the phenyl radical (C_6H_5) transient (*73*). Considering that GC-MS operated in an *off-line* mode only detects thermally stable species, Fischer et al. explored the high temperature (1,273 K) products of propargyl radical reactions in a molecular beam utilizing infrared/ultraviolet ion dip spectroscopy. The identification of not only benzene (C_6H_6), but also of naphthalene ($C_{10}H_8$), phenanthrene ($C_{14}H_{10}$), indene (C_9H_8), biphenyl ($C_{12}H_{10}$), and aromatics with acetylenic side chains documents unrestrained molecular mass growth processes due to higher-than-desired concentrations of propargyl radicals at levels of up to 7% (*79*). Whereas the foregoing studies nicely converged on the rates of the propargyl radical self-reaction, no consensus has been reached on the reaction mechanisms and the role of distinct isomers in the formation of the very first aromatic ring – benzene – under experimental conditions demanding an *in situ* analysis of the nascent reaction products and dilute radical concentrations excluding molecular mass growth products beyond benzene.

2. Products with Higher Mass-To-Charge Ratios

In our investigation, some aromatic hydrocarbon products beyond benzene at m/z = 102, 116, and 152 were detected only in the experiments with the bubbler temperature at 233 ± 1 K. These species are absent in the experiments when the bubbler was kept at 199 ± 1 K indicating that higher inlet concentrations of the precursor lead to undesired higher order reactions and mass growth processes beyond benzene. The PIE analysis was performed, and the results are visualized in Figs. S9-S11. Products at m/z = 102 are identified as phenylacetylene (C_6H_5CCH; Figure S9) and a second contributor. As benzocyclobutadiene can be produced via the reaction of benzyne and acetylene at elevated temperatures (*80*), and its adiabatic photoionization energy is 7.5 eV (*81*), benzocyclobutadiene likely contributes to signal at *m/z* = 102. Phenylacetylene is likely be the product from the reaction of the phenyl radical with acetylene followed by atomic hydrogen loss (*82*), while the reactant acetylene can be produced from the pyrolysis of benzene (*83*) or via the reaction of H atoms with methylacetylene (*84*). Phenyl was not detected in this work, but was predicted as a reactive intermediate. Species at m/z = 116 and 152 are indene (C_9H_8, Fig. S10) and acenaphthylene ($C_{12}H_8$, Fig. S11), respectively. Indene is a higher order reaction product from the combination of phenyl and propargyl, which was also reported in previous propargyl recombination studies (*79*). Pyrolysis of indene leads via H-loss to indenyl radical, which could further react with propargyl to yield acenaphthylene (*83*). The indenyl radical was not detected possibly due to the low concentration and the fast reaction with the high-concentration propargyl radical. Apart from these three higher aromatic hydrocarbons, two other species at m/z = 156, 158, 160 and 162 were observed (Figs. S12-S15). Considering their photoionization thresholds, molecular weights and relative intensities in mass spectra, these species are identified as bromobenzene ($C_6H_5{}^{79}Br$, 156 amu; $C_6H_5{}^{81}Br$, 158 amu) and molecular bromine ($^{79}Br_2$, 158 amu; $^{79}Br^{81}Br$, 160 amu; $^{81}Br_2$, 162 amu) from recombination of phenyl and atomic bromine, and atomic bromine self-recombination, respectively. The onsets of PIE curve at m/z = 156 and 158 appear at around 8.95 ± 0.05 eV, which agree well with the literature data of bromobenzene at 9.00 eV (*85*). The PIE curves at m/z = 158, 160 and 162 show a sharp increase around 10.5 eV. According to the photoionization energy of molecular bromine at 10.518 ± 0.003 eV (*86*), molecular bromine was detected due to high-harmonic VUV light from the light source. If the high-harmonic VUV is completely filtered, molecular bromine would be

undetectable at 10.5 eV. That is the reason why this species is absent in the results of the experiment performed under the condition with the bubbler at 233 K and pressure of 200 Torr).

3. Modeling

The computational model of the microreactor includes equations for the electric current and ohmic heating in the microreactor parts, equations for the moment, heat, and mass transfer for the gas flow inside the reactor, similar to the simulation by Guan et al. (*87*). The geometry of the microreactor used in the design model was as close as possible to the actual reactor. The microreactor includes copper, stainless steel, carbon electrodes solid parts. The temperature dependences of the physical properties of the materials from which the microreactor was made (SiC, graphite, stainless steel, copper) were taken into account. When modeling the gas flow, the Navier-Stokes equation was used together with the equations of heat and mass transfer with the corresponding boundary conditions. For the Naiver-Stokes equation, the following boundary conditions were used: the gas slip condition on the inner surface of the gas-flow channel of the microreactor was used in the form of Maxwell's model; the mass flow rate was set at the entrance to the microreactor; a pressure at the exit edge of the SiC tube was set such to provide the centerline Mach number 1. The following boundary conditions were used for the heat transfer equations: the gas temperature at the surface was equal to the surface temperature of the gas-flow channel of the microreactor; the gas temperature at the reactor inlet was taken equal to the room gas temperature of 297 K; convective heat removal was assumed at the SiC tube outlet edge. Heat release in chemical reactions was neglected. The electric power was adjusted to provide SiC temperature value measured in experiment. The computational model was solved with the COMSOL Multiphysics software package (*88*) under steady-state conditions. The calculated axial values of the pressure and temperature of the flow are shown in Fig. S16. Preheating of the gas flow in the gas-flow channel upstream from the SiC tube resulted in temperature near 400 K at the inlet to the SiC tube. Calculations did not show any substantial transverse variations in pressure and temperature, but the difference in the number densities of species at the centerline and near the wall of the SiC tube was about a factor of 2. In the electric heating zone, the centerline gas flow temperature differed from the SiC tube wall temperature by no more than 20

K in the transverse direction. The residence time of the gas in the heating zone of the reactor was about 140 μs, whereas the residence time of C_3H_3 radicals in the microreactor was about 90 μs. At gas flow rates of 38-60 ccm under the conditions of experiments 1-4, we have obtained an estimate of the Reynolds numbers Re>6 and Knudsen numbers <1. In the heating zone of the SiC tube the Mach number of the flow does not exceed 0.25. Thus, the "slip flow" approximation (*87*) used by us is valid for the heating zone of the SiC tube. Outside the electric heating zone, strong cooling of the SiC tube occurs due to heat transfer to the graphite electrodes and radiation cooling. In general, the spatial dependencies of the centerline gas-dynamic parameters (pressure, temperature, velocity) of the flow are qualitatively the same as those obtained in (*87*) for helium bulk gas. Naturally, some quantitative differences arise due to the design features of the microreactor and lower gas flow rate.

Table S1. Compilation of previous experimental results for C_6H_6 products and their branching ratios in the propargyl radical self-reaction.

Groups	1,5-Hexdiyne	1,2,4,5-Hexatetraene	3,4-Dimethylene-cyclobutene	Fulvene	1,2-Hexadiene-5-yne	2-Ethynyl-1,3-butadiene	*cis*-1,3-Hexadiene-5-yne	*trans*-1,3-Hexadiene-5-yne	Benzene
Fahr and Nayak(*69*)	Y 0.60				Y 0.25				
Scherer et al. (*71*)	Y								Y
Shafir et al.(*73*)	Y 0.31(500K) 0.19(700K) 0.04(900K) 0.04(1000K) 0.01(1100K)			Y 0(500K) 0(700K) 0.09(900K) 0.06(1000K) 0.07(1100K)					Y 0.26(500K) 0.30(700K) 0.82(900K) 0.85(1000K) 0.87(1100K)
Howe and Fahr(*70*)	Y 0.4(27mbar^{ae}) 0.42(67mbar^{ae}) 0.4(133mbar^{ae}) 0.44(332mbar^{ae}) 0.48(600mbar^{ae}) 0.507(933mbar^{ae}) 0.345(27mbar^{be}) 0.39(67mbar^{be}) 0.43(133mbar^{be}) 0.43(332mbar^{be}) 0.465(600mbar^{be}) 0.47(933mbar^{be}) 0.265(27mbar^{ce}) 0.31(67mbar^{ce}) 0.368(133mbar^{ce}) 0.38(332mbar^{ce}) 0.43(600mbar^{ce}) 0.455(933mbar^{ce}) 0.47(27mbar^{af}) 0.485(133mbar^{af}) 0.46(332mbar^{af}) 0.545(933mbar^{af}) 0.39(27mbar^{bf}) 0.405(133mbar^{bf}) 0.475(933mbar^{bf}) 0.27(27mbar^{cf}) 0.375(133mbar^{cf}) 0.45(933mbar^{cf}) 0.01(27mbar^{df}) 0.04(67mbar^{df}) 0.03(133mbar^{df}) 0.082(332mbar^{df})		Y 0.13(27mbar^{ae}) 0.115(67mbar^{ae}) 0.15(133mbar^{ae}) 0.125(332mbar^{ae}) 0.115(600mbar^{ae}) 0.1(933mbar^{ae}) 0.15(27mbar^{be}) 0.115(67mbar^{be}) 0.104(133mbar^{be}) 0.114(332mbar^{be}) 0.08(600mbar^{be}) 0.07(933mbar^{be}) 0.27(27mbar^{ce}) 0.28(67mbar^{ce}) 0.23(133mbar^{ce}) 0.215(332mbar^{ce}) 0.17(600mbar^{ce}) 0.14(933mbar^{ce}) 0.10(27mbar^{af}) 0.095(133mbar^{af}) 0.11(332mbar^{af}) 0.06(933mbar^{af}) 0.20(27mbar^{bf}) 0.185(133mbar^{bf}) 0.105(933mbar^{bf}) 0.31(27mbar^{cf}) 0.27(133mbar^{cf}) 0.165(933mbar^{cf}) 0.525(27mbar^{df}) 0.72(67mbar^{df}) 0.86(133mbar^{df}) 0.79(332mbar^{df})	Y 0.02(27mbar^{ae}) 0.01(67mbar^{ae}) 0.006(133mbar^{ae}) 0.005(332mbar^{ae}) 0.004(600mbar^{ae}) 0.003(933mbar^{ae}) 0.005(27mbar^{be}) 0.005(67mbar^{be}) 0.001(133mbar^{be}) 0.001(332mbar^{be}) 0(600mbar^{be}) 0(933mbar^{be}) 0.005(27mbar^{ce}) 0.002(67mbar^{ce}) 0.002(133mbar^{ce}) 0(332mbar^{ce}) 0.001(600mbar^{ce}) 0.001(933mbar^{ce}) 0.01(27mbar^{af}) 0.005(133mbar^{af}) 0.005(332mbar^{af}) 0.005(933mbar^{af}) 0.005(27mbar^{bf}) 0.005(133mbar^{bf}) 0.005(933mbar^{bf}) 0.015(27mbar^{cf}) 0.01(133mbar^{cf}) 0.01(933mbar^{cf}) 0.015(27mbar^{df}) 0.013(67mbar^{df}) 0.01(133mbar^{df}) 0.008(332mbar^{df})	Y 0.335(27mbar^{ae}) 0.365(67mbar^{ae}) 0.4(133mbar^{ae}) 0.415(332mbar^{ae}) 0.4(600mbar^{ae}) 0.38(933mbar^{ae}) 0.325(27mbar^{be}) 0.37(67mbar^{be}) 0.41(133mbar^{be}) 0.43(332mbar^{be}) 0.425(600mbar^{be}) 0.43(933mbar^{be}) 0.21(27mbar^{ce}) 0.3(67mbar^{ce}) 0.35(133mbar^{ce}) 0.375(332mbar^{ce}) 0.38(600mbar^{ce}) 0.364(933mbar^{ce}) 0.345(27mbar^{af}) 0.40(133mbar^{af}) 0.41(332mbar^{af}) 0.38(933mbar^{af}) 0.32(27mbar^{bf}) 0.39(133mbar^{bf}) 0.39(933mbar^{bf}) 0.215(27mbar^{cf}) 0.325(133mbar^{cf}) 0.36(933mbar^{cf}) 0.02(27mbar^{df}) 0.027(67mbar^{df}) 0.03(133mbar^{df}) 0.06(332mbar^{df})				Y 0.12(27mbar^{ae}) 0.09(67mbar^{ae}) 0.04(133mbar^{ae}) 0.015(332mbar^{ae}) 0.05(600mbar^{ae}) 0.01(933mbar^{ae}) 0.175(27mbar^{be}) 0.12(67mbar^{be}) 0.055(133mbar^{be}) 0.025(332mbar^{be}) 0.03(600mbar^{be}) 0.03(933mbar^{be}) 0.25(27mbar^{ce}) 0.108(67mbar^{ce}) 0.05(133mbar^{ce}) 0.03(332mbar^{ce}) 0.019(600mbar^{ce}) 0.04(933mbar^{ce}) 0.075(27mbar^{af}) 0.015(133mbar^{af}) 0.015(332mbar^{af}) 0.01(933mbar^{af}) 0.085(27mbar^{bf}) 0.015(133mbar^{bf}) 0.025(933mbar^{bf}) 0.19(27mbar^{cf}) 0.02(133mbar^{cf}) 0.015(933mbar^{cf}) 0.43(27mbar^{df}) 0.20(67mbar^{df}) 0.07(133mbar^{df}) 0.06(332mbar^{df})

	0.22(600mbar[df]) 0.27(933mbar[df])		0.555(600mbar[df]) 0.475(933mbar[df])	0.01(600mbar[df]) 0.009(933mbar[df])	0.14(600mbar[df]) 0.216(933mbar[df])				0.075(600mbar[df]) 0.03(933mbar[df])
Brezinsky et al.[g] (*77*)	Y	Y	Y	Y	Y	Y			Y
Osborn et al.(*78*)	Y 0.45(5mbar) 0.55(10mbar)	Y 0.004(5mbar) 0(10mbar)	Y 0.006(5mbar) 0(10mbar)	Y 0.006(5mbar) 0.01(10mbar)	Y 0.24(5mbar) 0.14(10mbar)	Y 0.12(5mbar) 0.04(10mbarr)	Y 0.011(5mbar) 0.01(10mbar)	Y 0.007(5mbar) 0.01(10mbar)	Y 0.15(5mbar) 0.24(10mbar)
Rijs et al.(*79*)									Y

Note: [a.]295 K; [b.]398 K; [c.]523 K; [d.] 623K;

[e.] These branching ratios were determined from the experiment with the 248 nm photolysis of mixtures of C_3H_3Br/He.

[f.] These branching ratios were determined from the experiment with the 193 nm photolysis of mixtures of C_3H_3Cl/He.

[g.] Branching ratios are temperature- and pressure-dependent.

Table S2. Conditions in the present experiments.

	Propargyl Bromide Bath temperature (K)	Total Inlet Pressure (Torr)	Partial pressure of C_3H_3Br (Torr)	Reactor temperature (K)	Initial mole fraction of C_3H_3Br
1	199 ± 1	200 ± 5	2.0 ± 0.2	1343 ± 10	1.0%
2	199 ± 1	300 ± 5	2.0 ± 0.2	1273 ± 10	0.7%
3	233 ± 1	200 ± 5	9.6 ± 0.5	1273 ± 10	4.8%
4	233 ± 1	300 ± 5	9.6 ± 0.5	1273 ± 10	3.2%

Table S3. Branching ratios of the hydrocarbons derived in the present studies.

	Allene (*89*)	Methylacetylene (*90*)	Benzyne	Benzene (*90*)	Fulvene (*78*)	1,5-Hexadiyne (*78*)	2-Ethynyl-1,3-butadiene (*78*)
199K/200Torr (1%)	0.239 (0.191, 0.287)	0.358 (0.286, 0.430)	0.035 (0.018, 0.070)	0.084 (0.067, 0.101)	0.033 (0.017, 0.066)	0.050 (0.040, 0.060)	0.201 (0.101, 0.402)
modeled	0.236 (0.201, 0.271)	0.357 (0.303, 0.411)	0.023 (0.020, 0.026)	0.087 (0.074, 0.100)	0.035 (0.030, 0.040)	0.050 (0.043, 0.058)	0.212 (0.180, 0.244)
199K/300Torr (0.7%)	0.188 (0.150, 0.226)	0.377 (0.302, 0.452)	0.040 (0.020, 0.080)	0.075 (0.060, 0.090)	0.038 (0.019, 0.076)	0.056 (0.045, 0.067)	0.226 (0.113, 0.452)
modeled	0.202 (0.172, 0.232)	0.309 (0.263, 0.355)	0.046 (0.039, 0.053)	0.085 (0.072, 0.098)	0.037 (0.031, 0.043)	0.063 (0.054, 0.072)	0.258 (0.219, 0.297)
233K/200Torr (4.8%)	0.076 (0.061, 0.091)	0.152 (0.122, 0.182)	0.285 (0.143, 0.570)	0.076 (0.061, 0.091)	0.068 (0.034, 0.136)	0.114 (0.091, 0.137)	0.228 (0.114, 0.456)
233K/300Torr (3.2%)	0.075 (0.060, 0.090)	0.100 (0.080, 0.120)	0.225 (0.113, 0.450)	0.090 (0.072, 0.108)	0.060 (0.030, 0.120)	0.150 (0.120, 0.180)	0.300 (0.150, 0.600)

Note: The temperatures and pressures exhibited in the first column represent the temperatures of the bubbler and the inlet pressures. Detailed experiment conditions are listed in Table S2. The values in the parenthesis determine the lower and upper error limits for the experimental branching ratios. The references labelled after each species present the sources of photoionization cross sections. The photoionization cross section of benzyne was estimated and taken from reference (*45*). For the measured photoionization cross sections (allene, methylacetylene, benzene and 1,5-hexadiyne), the uncertainty of their branching ratios is ± 20% while as the photoionization cross sections of benzyne, fulvene and 2-ethynyl-1,3-butadiene are estimated or theoretically calculated, the uncertainty is proposed to be a factor of 2 (*90*).

Table S4. List of rate constants and modified rate constants used in the simulations in units of $cm^3\ s^{-1}\ mol^{-1}$ and s^{-1} for bimolecular and unimolecular reactions, respectively.

	Nominal Rate Constants	**Correction factors for modified rate constants**
	Reaction R1 $HCCCH_2Br \leftrightarrows C_3H_3 + Br$[a]	
k1f	6.618e8*exp(-19285.23/T)*p/(1+p*(-0.0136+0.00665*exp(2221.19/T)))	×1.3×exp(3000/T)
k1r	(-6.26+0.3949*exp(4542.1/T))*1e-14*p/(1+0.01*p*(-1.453+0.697*exp(2188.62/T)))*6e23	×1
	Reaction R2a $C_3H_3 + H \leftrightarrows C_3H_4$(propyne)	
k2afp1[b]	10^36.56*T^(-7.36)*exp(-6039/1.987/T)	×2
k2afp2[b]	10^29.90*T^(-5.06)*exp(-4861/1.987/T)	×2
k2ar[c]	7.8e-6*exp(-335000/8.314472/T)*6.022e23	×1
	Reaction R2b $C_3H_3 + H \leftrightarrows C_3H_4$(allene)	
k2bfp1[b]	10^36.53×T^(-7.41)×exp(-6337/1.987/T)	×2
k2bfp2[b]	10^29.50×T^(-5.00)×exp(-4711/1.987/T)	×2
k2br[c]	3.32e-6*exp(-335000/8.314472/T)*6.022e23	×1
	Reaction R3 $C_3H_3 + C_3H_3 \leftrightarrows C_6H_5 + H$[d]	
k3fp1	4.31E+64*T^(-15.107)*exp(-31700/1.987/T) + 2.87E+35*T^(-6.8136)*exp(-13327/1.987/T)	×1
k3fp2	2.47E+66*T^(-15.446)*exp(-36606/1.987/T) + 1.74E+35*T^(-6.7033)*exp(-15756/1.987/T)	×1
k3fp3	1.64E+64*T^(-14.71)*exp(-38110/1.987/T) + 8.00E+32*T^(-6.0398)*exp(-16226/1.987/T)	×1
k3rp1	2.73E+64*T^(-13.363)*exp(-61451/1.987/T) + 7.91E+127*T^(-29.259)*exp(-1.73E+05/1.987/T)	×1
k3rp2	6.69E+63*T^(-13.074)*exp(-64307/1.987/T)	×1
k3rp3	9.98E+79*T^(-17.577)*exp(-78756/1.987/T) + 2.07E+43*T^(-7.4005)*exp(-52240/1.987/T)	×1
	Reaction R4a $C_3H_3 + C_3H_3 \rightarrow C_6H_6$(benzene)[d]	
k4afp1	1.19E+137*T^(-35.905)*exp(-81665/1.987/T) + 6.87E+66*T^(-16.626)*exp(-21855/1.987/T)	×0.1
k4afp2	1.97E+103*T^(26.285)*exp(-56243/1.987/T) + 1.84E+66*T^(-16.364)*exp(-23047/1.987/T)	×0.1
k4afp3	-4.85E+98*T^(-25.281)*exp(-43301/1.987/T) + 5.24E+82*T^(-20.606)*exp(-34270/1.987/T)	×0.1
	Reaction R4b $C_3H_3 + C_3H_3 \rightarrow C_6H_6$(fulvene)[d]	
k4bfp1	1.92E+87*T^(-22.384)*exp(-37245/1.987/T) + 1.13E+56*T^(-13.82)*exp(-13512/1.987/T)	×0.067
k4bfp2	3.86E+83*T^(-21.017)*exp(-37704/1.987/T) + 5.28E+58*T^(-14.451)*exp(-15599/1.987/T)	×0.067
k4bfp3	2.09E+82*T^(-20.496)*exp(-38166/1.987/T) + 3.61E+58*T^(-14.342)*exp(-15974/1.987/T)	×0.067
	Reaction R4c $C_3H_3 + C_3H_3 \rightarrow C_6H_6$(1,5-hexadiyne)[d]	
k4cfp1	1.76E+78*T^(-20.37)*exp(-32169/1.987/T) + 5.51E+54*T^(-14.137)*exp(-12026/1.987/T)	×6

k4cfp2	2.64E+61*T^(-15.268)*exp(-22502/1.987/T) + 2.79E+47*T^(-11.604)*exp(-9628.5/1.987/T)	×6
k4cfp3	8.78E+85*T^(-22.118)*exp(-38540/1.987/T) + 2.00E+55*T^(-13.801)*exp(-13257/1.987/T)	×6
	Reaction R4d $C_3H_3 + C_3H_3 \leftrightarrows C_6H_6$(2-ethynyl-1,3-butadiene)[d]	
k4dfp1	4.00E+84*T^(-21.527)*exp(-35767/1.987/T) + 1.89E+60*T^(-15.09)*exp(-15352/1.987/T)	×0.625
k4dfp2	5.36E+82*T^(-20.74)*exp(-37229/1.987/T) + 2.88E+55*T^(-13.495)*exp(-14159/1.987/T)	×0.625
k4dfp3	7.41E+79*T^(-19.783)*exp(-37027/1.987/T) + 4.92E+51*T^(-12.286)*exp(-13002/1.987/T)	×0.625
k4drp1	8.77E+33*T^(-6.0712)*exp(-71073/1.987/T)	×2
k4drp2	6.12E+29*T^(-4.8273)*exp(-67162/1.987/T)	×2
k4drp3	4.30E+39*T^(-7.6343)*exp(-71997/1.987/T)	×2
	Reaction R5a C_6H_6(1,5-hexadiyne) → C_6H_6(fulvene)[d]	
k5afp1	1.40E+75*T^(-19.544)*exp(-52706/1.987/T)	×0
k5afp2	23.40E+61*T^(-15.232)*exp(-48101/1.987/T)	×0
k5afp3	1.48E+63*T^(-15.611)*exp(-49730/1.987/T)	×0
	Reaction R5b C_6H_6(1,5-hexadiyne) → C_6H_6(benzene)[d]	
k5bfp1	9.48E-55*T^(17.136)*exp(18644/1.987/T) + 6.68E+76*T^(-19.007)*exp(-79650/1.987/T)	×0
k5bfp2	2.86E+41*T^(-8.7)*exp(-59368/1.987/T)	×0
k5bfp3	1.48E+50*T^(-10.994)*exp(-68465/1.987/T)	×0
	Reaction R6a C_6H_6(fulvene) → C_6H_6(benzene)[d]	
k6afp1	1.56E+87*T^(-21.086)*exp(-1.22E+05/1.987/T)	×1
k6afp2	1.13E+77*T^(-18.082)*exp(-1.17E+05/1.987/T)	×1
k6afp3	7.56E+87*T^(-21.796)*exp(-1.15E+05/1.987/T) + 1.17E+99*T^(-23.891)*exp(-1.41E+05/1.987/T)	×1
k6arp1	5.36E+87*T^(-20.781)*exp(-1.53E+05/1.987/T)	×1
k6arp2	6.72E+78*T^(-18.115)*exp(-1.49E+05/1.987/T)	×1
k6arp3	1.48E+90*T^(-21.905)*exp(-1.49E+05/1.987/T) + 5.55E+104*T^(-24.972)*exp(-1.77E+05/1.987/T)	×1
	Reaction R6b C_6H_6(fulvene) ⇆ C_6H_5 + H[d]	
k6bfp1	1.34E+91*T^(-21.678)*exp(-1.42E+05/1.987/T)	×1
k6bfp2	1.13E+89*T^(-20.863)*exp(-1.45E+05/1.987/T)	×1
k6bfp3	1.19E+87*T^(-20.178)*exp(-1.47E+05/1.987/T)	×1
k6brp1	2.64E+45*T^(-9.6881)*exp(-23255/1.987/T) + 2.96E+87*T^(-20.902)*exp(-57167/1.987/T)	×1
k6brp2	3.08E+35*T^(-6.6861)*exp(-20378/1.987/T) + 3.91E+83*T^(-19.584)*exp(-59105/1.987/T)	×1
k6brp3	2.75E+32*T^(-5.8045)*exp(-19675/1.987/T) + 5.24E+83*T^(-19.488)*exp(-62324/1.987/T)	×1
	Reaction R7 C_6H_5 +H ⇆ C_6H_6(benzene)[d]	
k7fp1	4.63E+85*T^(-20.439)*exp(-48256/1.987/T) + 5.51E+43*T^(-9.1968)*exp(-11284/1.987/T)	×0.1

k7fp2	2.90E+85*T^(-20.207)*exp(-50909/1.987/T) + 5.09E+41*T^(-8.5303)*exp(-10766/1.987/T)	×0.1
k7fp3	4.63E+85*T^(-20.138)*exp(-53321/1.987/T) + 2.08E+39*T^(-7.7679)*exp(-10025/1.987/T)	×0.1
k7rp1	-3.03E+71*T^(-15.07)*exp(-1.69E+05/1.987/T) + 2.10E+43*T^(-7.7577)*exp(-1.31E+05/1.987/T)	×1
k7rp2	2.00E+75*T^(-16.775)*exp(-1.54E+05/1.987/T)	×1
k7rp3	9.93E+77*T^(-17.918)*exp(-1.50E+05/1.987/T) + 2.65E+101*T^(-23.651)*exp(-1.84E+05/1.987/T)	×1
	Reaction R17a C_6H_6(2-ethynyl-1,3-butadiene) → C_6H_6(fulvene)[d]	
k17ap1	1.60E+93*T^(-23.531)*exp(-1.04E+05/1.987/T)	×1
k17ap2	4.99E+79*T^(-19.546)*exp(-96150/1.987/T)	×1
k17ap3	3.80E+75*T^(-18.255)*exp(-94952/1.987/T)	×1
	Reaction R17b C_6H_6(2-ethynyl-1,3-butadiene) → C_6H_6(benzene)[d]	
k17bp1	2.15E+111*T^(-28.284)*exp(-1.25E+05/1.987/T)	×1
k17bp2	3.80E+114*T^(-28.906)*exp(-1.33E+05/1.987/T)	×1
k17bp3	2.40E+100*T^(-24.769)*exp(-1.26E+05/1.987/T)	×1
	Reaction R17c C_6H_6(2-ethynyl-1,3-butadiene) → C_6H_5 + H[d]	
k17cp1	5.61E+88*T^(-21.621)*exp(-1.16E+05/1.987/T)	×1
k17cp2	8.01E+87*T^(-21.162)*exp(-1.21E+05/1.987/T)	×1
k17cp3	6.84E+90*T^(-21.836)*exp(-1.28E+05/1.987/T)	×1
	Reaction R8 C_6H_6 + H ⇆ C_6H_5 + H_2[e]	
k8f	4.57e8*T^1.88*exp(-14839/1.987/T)	×1
k8r	1.69e4*T^2.64*exp(-4559/1.987/T)	×1
	Reaction R9 C_6H_6(fulvene) + H ⇆ C_6H_6(benzene) + H[f]	
k9f	6.54e25*T^(-2.8332)*exp(-43768/1.987/T)	×1
k9r	1.09e25*T^(-3.0678)*exp(-11761/1.987/T)	×0.2
	Reaction R10 C_6H_5 ⇆ o-C_6H_4 (or l-C_6H_4) + H[g]	
k10f	7.99*1e41*T^(-7.72)*exp(-40000/T)+3.32*1e73*T^(-16.02)*exp(-60000/T))	×1
k10r	6.59E+80*T^(-19.24)*exp(-41380.0/1.987/T)+1.34E+48*T^(-10.56)*exp(-12820.0/1.987/T)	×1
	Reaction R11 C_6H_5Br ⇆ C_6H_5 + Br[h]	
k11fp1	0.20182E+112*T^(-26.899)*exp(-77372/T)+0.79938E+70*T^(-16.473)*exp(-51627/T)	×1
k11fp3	0.41271E+102*T^(-24.083)*exp(-74861/T)+0.91502E+61*T^(-13.762)*exp(-49757/T)	×1
k11rp1	0.20355E+47*6.02E+23*T^(-16.224)*exp(-19076/T)+0.24889E+07*6.02E+23*T^(-5.2016)*exp(-2835.3/T)	×1
k11rp3	0.52087E+12*6.02E+23*T^(-6.3557)*exp(-7644.6/T)+2.9856*6.02E+23*T^(-3.4051)*exp(-1596.9/T)	×1
	Reaction R12 C_6H_5 + Br → C_6H_4 + HBr[i]	
k12	2.74*1e-13*T^0.490*exp(-10630/1.987/T)*6E23	×1
	Reaction R13 C_6H_5 + H → C_6H_4 + H_2[i]	

k13	2.74*1e-13*T^0.490*exp(-10630/1.987/T)*6E23	×1
	Reaction R14 **$C_6H_5 + C_6H_5 \rightarrow C_{12}H_{10}$**[j]	
k14	10^22.508*T^(-2.81)*exp(-2410/T)	×1
	Reaction R15 **$C_6H_5 + C_6H_5 \rightarrow C_6H_6 + C_6H_4$(all isomers)**[j]	
k15	3e12	×1
	Reaction R16 **$C_3H_3 + C_6H_5 \rightarrow C_9H_8$**[k]	
k16	6e13	×1

[a]From VRC-TST calculations in the present study. [b]From Ref. (*91*). [c]From Ref. (*92*). [d]The rate constants were computed using the C_6H_6 potential energy surface, energies, and molecular parameters from Ref. (*31*) using the same RRKM-ME approach and collisional parameters. The changes made in the high-pressure limit $C_3H_3 + C_3H_3$ and $C_6H_5 + H$ rate constants and the modifications used in the lumped mechanism are described in the text. [e]From Ref. (*93*). [f]From Ref. (*94*). [g]From Ref. (*95*). [h]Adopted from the $C_{10}H_7Br \leftrightarrows C_{10}H_7 + Br$ rate constants from Ref. (*48*). [i]Adopted from the rate constant of the disproportionation reaction of styrenyl radical with H producing phenylacetylene + H_2 in Ref. (*96*). [j]From Ref. (*97*). [k]From Ref. (*98*).

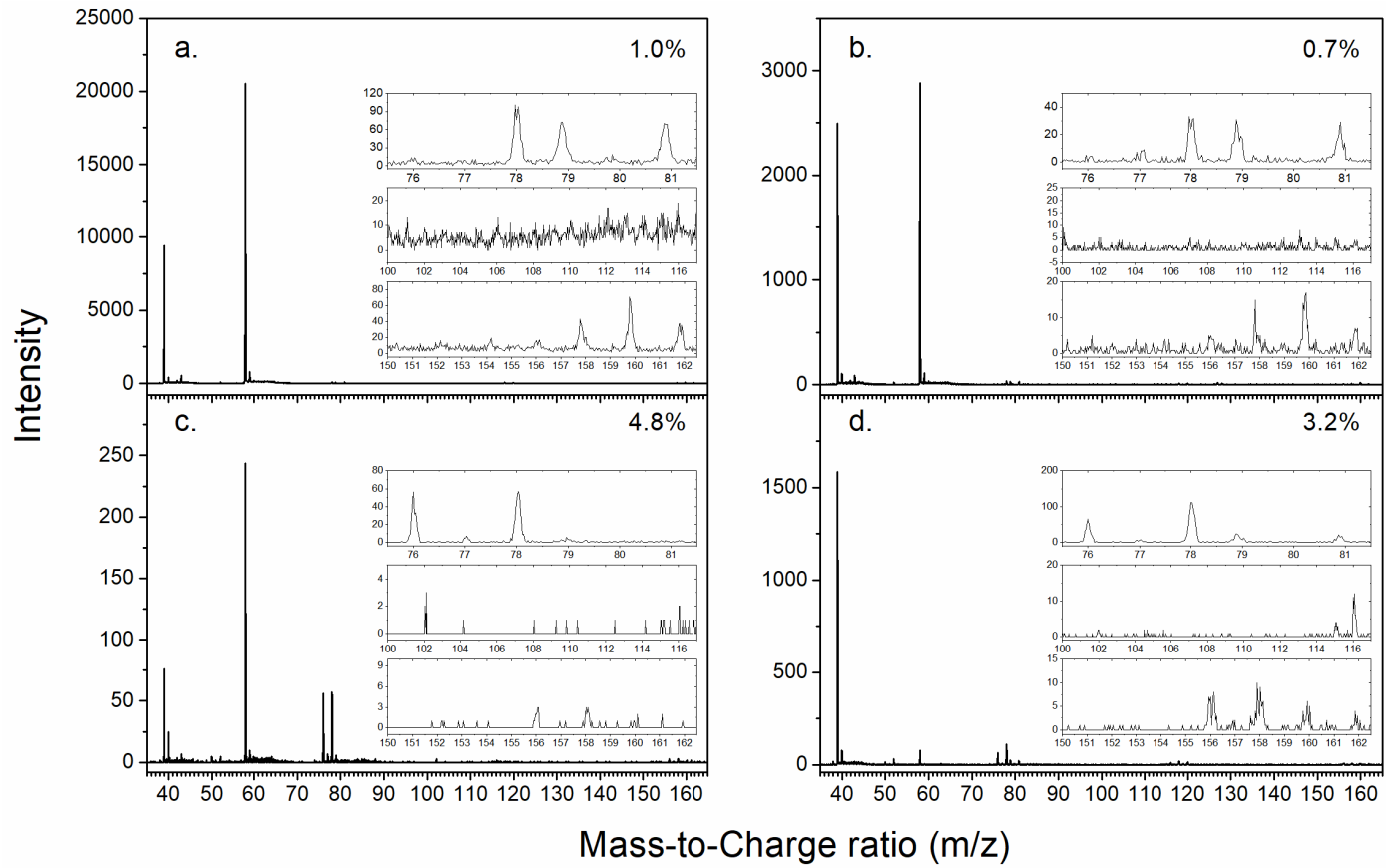

Figure S1. Comparison of the mass spectra for the propargyl recombination systems recorded at 10.5 eV at different experiment conditions. The percentages exhibited in the figures represent the initial mole fractions of propargyl bromide (C_3H_3Br). Detailed experiment conditions are listed in Table S2. The signal at m/z = 58 defines acetone along with its fragment at m/z = 43. Acetone is the residue from the previous cleaning of the main chamber. Thus, no acetone was in the reactor and it is not involved in the reaction.

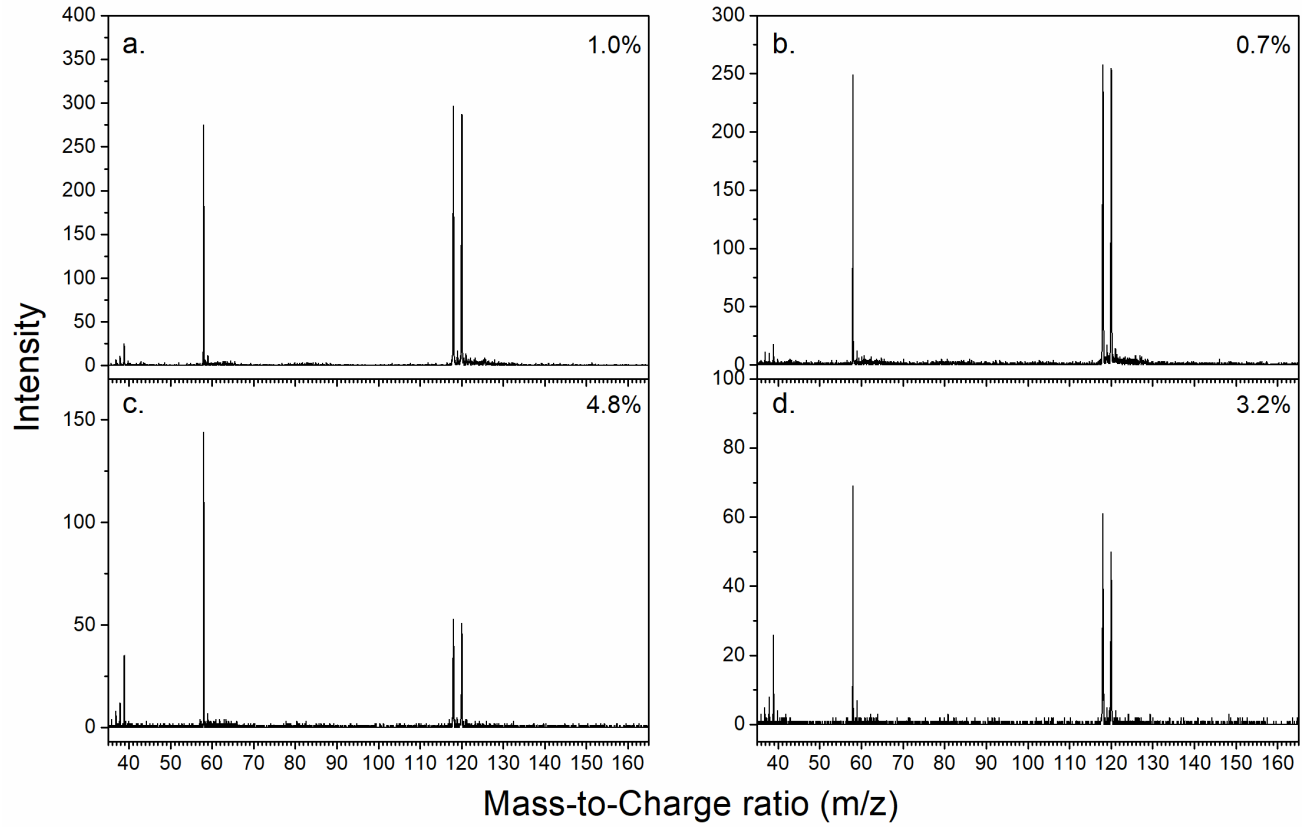

Figure S2. Comparison of the mass spectra for propargylbromide-helium recorded at different experiment conditions with the reactor at room temperature. The percentages exhibited in the figures represent the initial mole fractions of propargyl bromide (C_3H_3Br). Detailed experiment conditions are listed in Table S2. The signal at m/z = 58 defines acetone along with its fragment at m/z = 43. Acetone is the residue from the previous cleaning of the main chamber. Thus, no acetone was in the reactor and it is not involved in the reaction. Comparative peaks at m/z = 118 and 120 represent the precursor $C_3H_3{}^{79}Br$ and $C_3H_3{}^{81}Br$. The fragmentation of the precursor leads to the signal visible at m/z = 37 to 39.

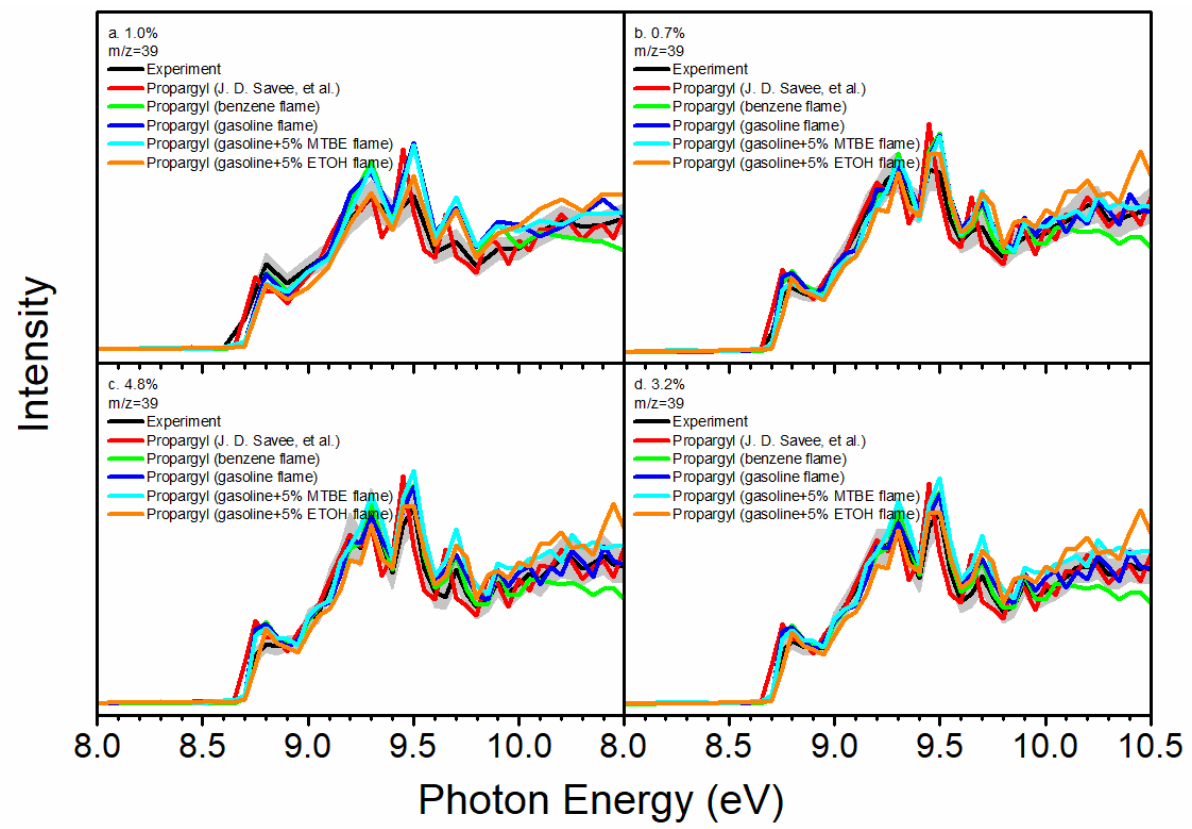

Figure S3. Photoionization efficiency (PIE) curves for signal at *m/z* = 39 in the propargyl recombination system. Black: experimentally derived PIE curves; Colored lines: reference PIE curves (*47*,*99*). The percentages exhibited in the figures represent the initial mole fractions of propargyl bromide (C_3H_3Br). Detailed experiment conditions are listed in Table S2.

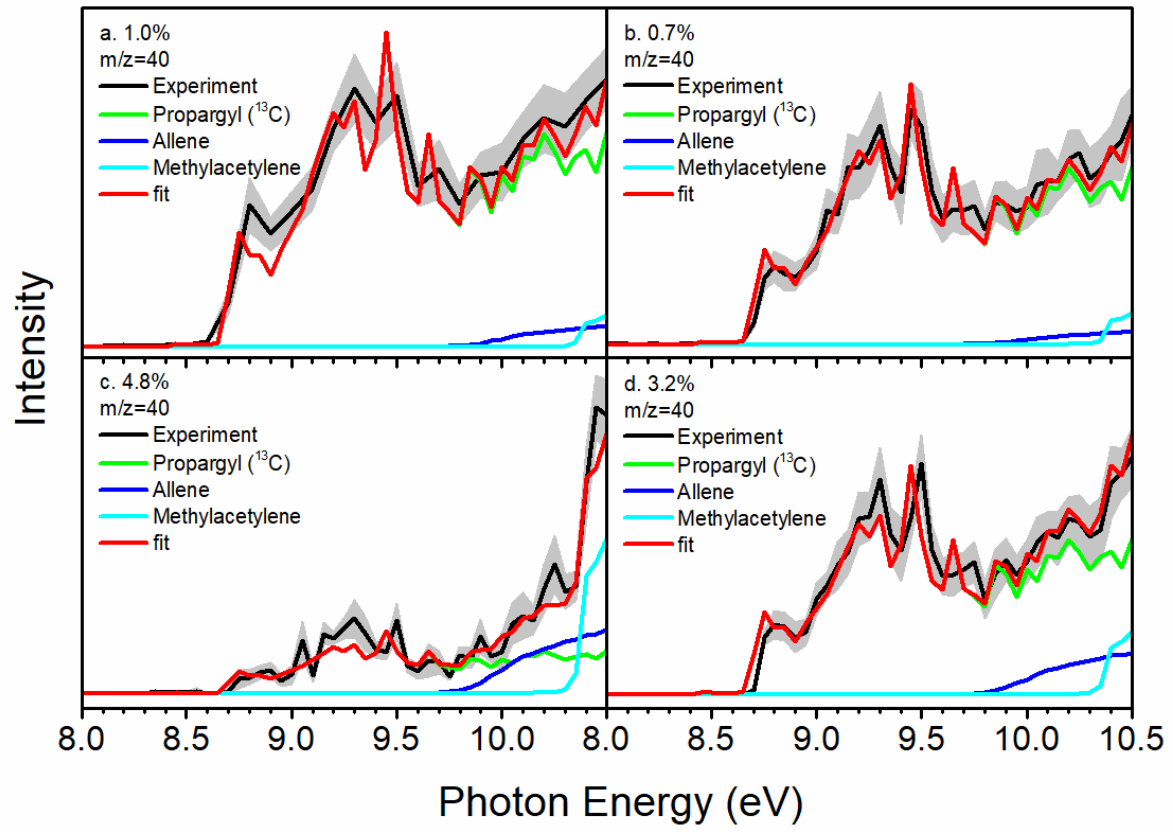

Figure S4. Photoionization efficiency (PIE) curves for signal at *m/z* = 40 in the propargyl recombination system. Black: experimentally derived PIE curves; colored lines (green, blue and cyan): reference PIE curves; red lines: overall fit. The percentages exhibited in the figures represent the initial mole fractions of propargyl bromide (C_3H_3Br). Detailed experiment conditions are listed in Table S2.

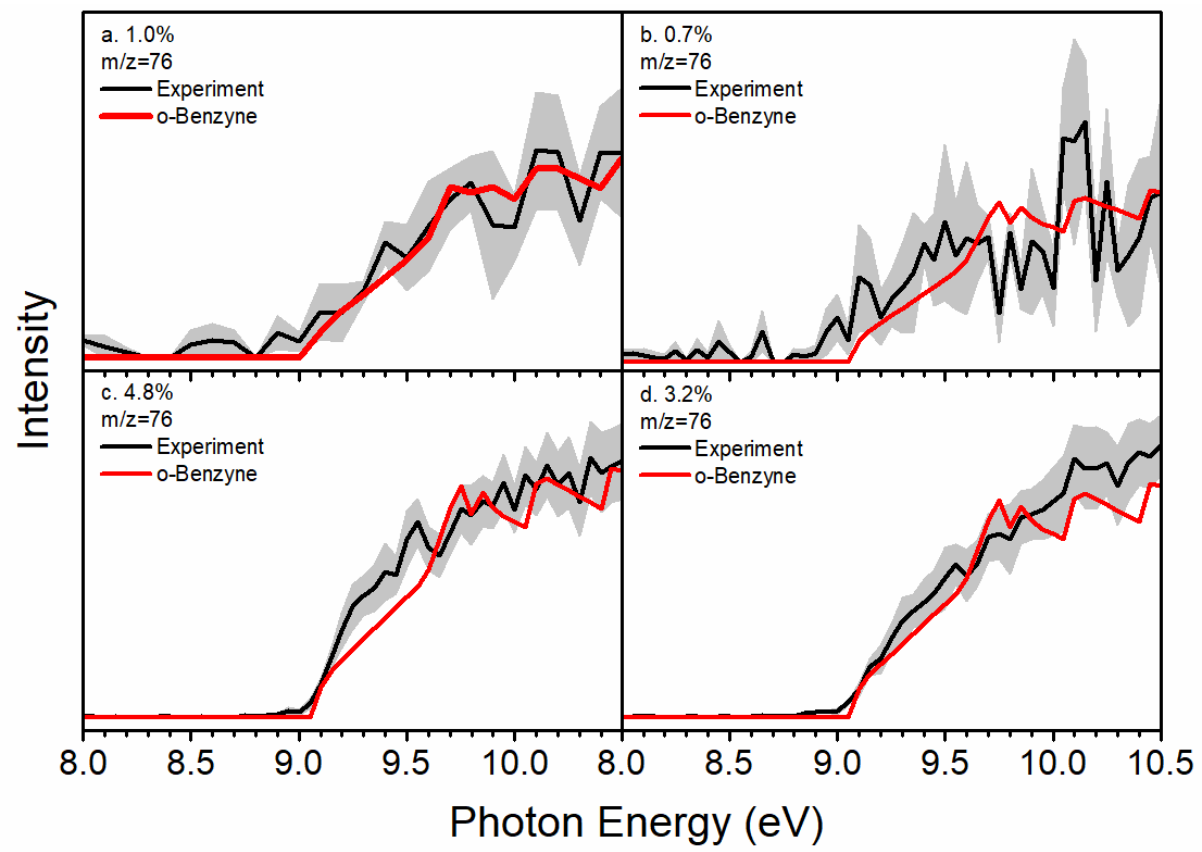

Figure S5. Photoionization efficiency (PIE) curves for signal at *m/z* = 76 in the propargyl recombination system. Black: experimentally derived PIE curves; red lines: reference PIE curves. The percentages exhibited in the figures represent the initial mole fractions of propargyl bromide (C_3H_3Br). Detailed experiment conditions are listed in Table S2.

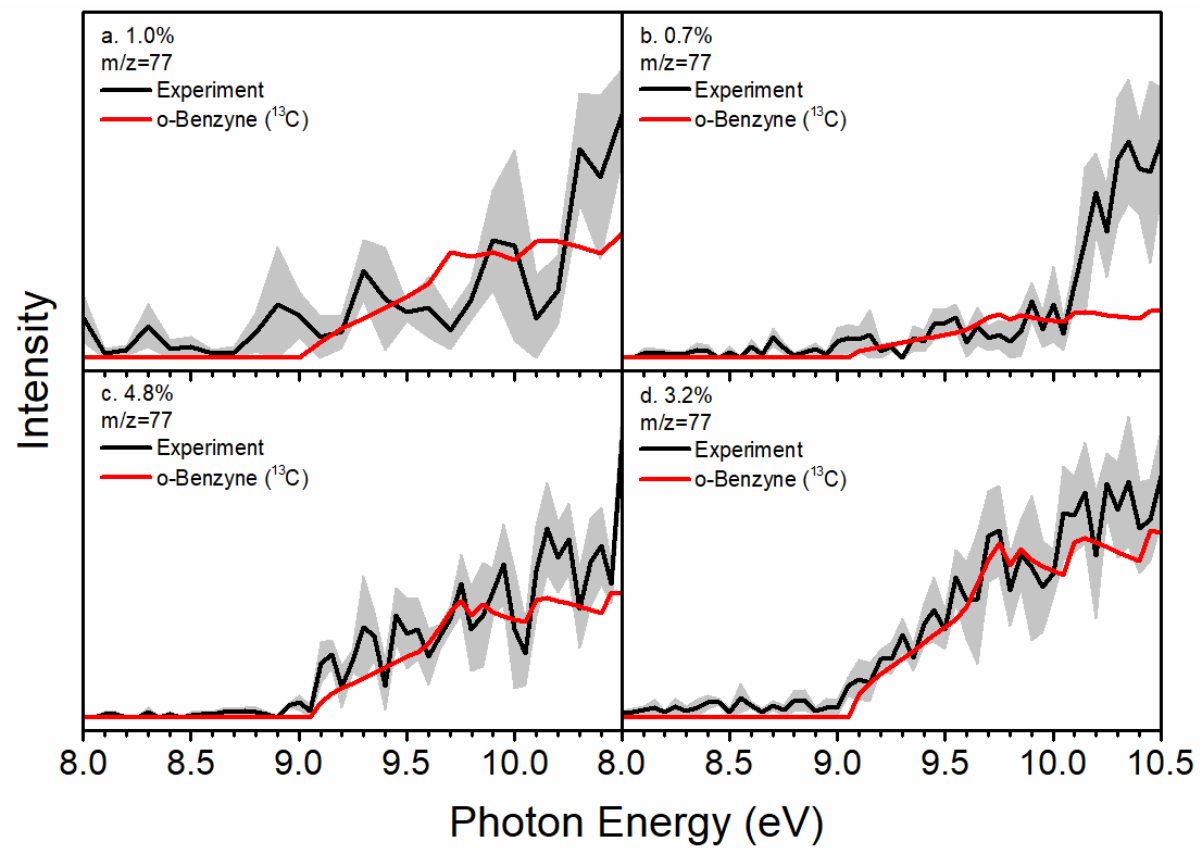

Figure S6. Photoionization efficiency (PIE) curves for signal at *m/z* = 77 in the propargyl recombination system. Black: experimentally derived PIE curves; red lines: reference PIE curves. The percentages exhibited in the figures represent the initial mole fractions of propargyl bromide (C_3H_3Br). Detailed experiment conditions are listed in Table S2.

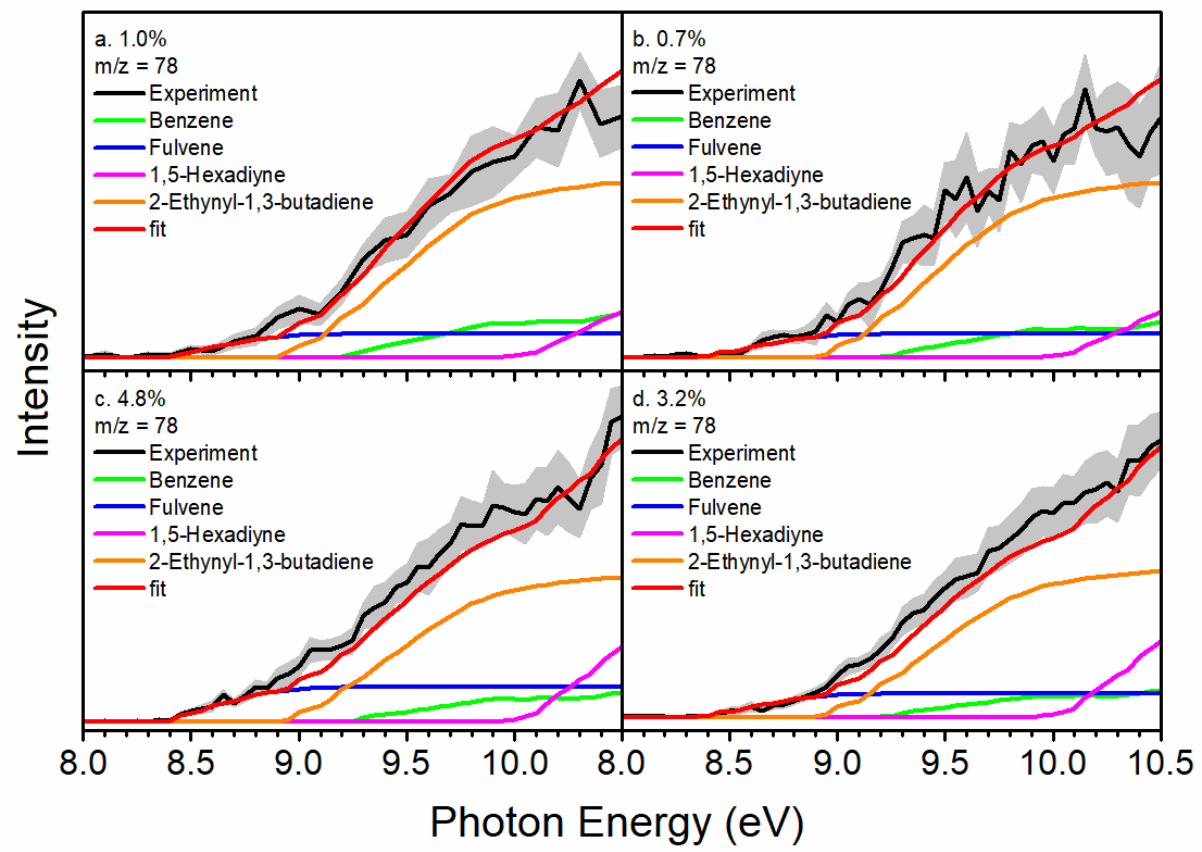

Figure S7. Photoionization efficiency (PIE) curves for signal at *m/z* = 78 in the propargyl recombination system. Black: experimentally derived PIE curves; colored lines (green, blue, purple and orange): reference PIE curves; red lines: overall fit. The percentages exhibited in the figures represent the initial mole fractions of propargyl bromide (C_3H_3Br). Detailed experiment conditions are listed in Table S2.

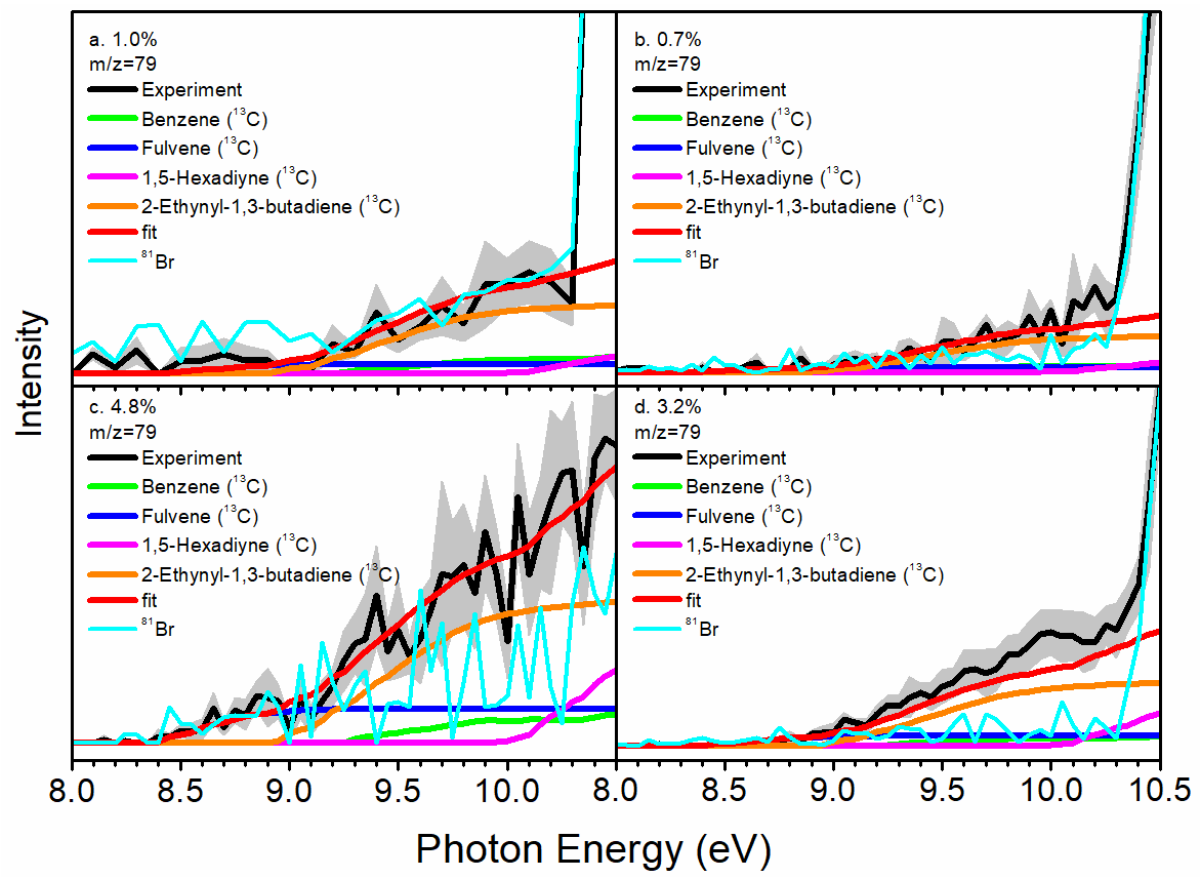

Figure S8. Photoionization efficiency (PIE) curves for signal at *m/z* = 79 in the propargyl recombination system. Black: experimentally derived PIE curves; colored lines (green, blue, purple and orange): reference PIE curves; red lines: overall fit. The percentages exhibited in the figures represent the initial mole fractions of propargyl bromide (C_3H_3Br). Detailed experiment conditions are listed in Table S2. For the onsets at 10.30 eV, the signal might be contributed from the photoionization of atomic bromine induced by high-harmonic VUV light. The dark yellow dashed line presents the PIE curve for *m/z* = 81 observed in this work.

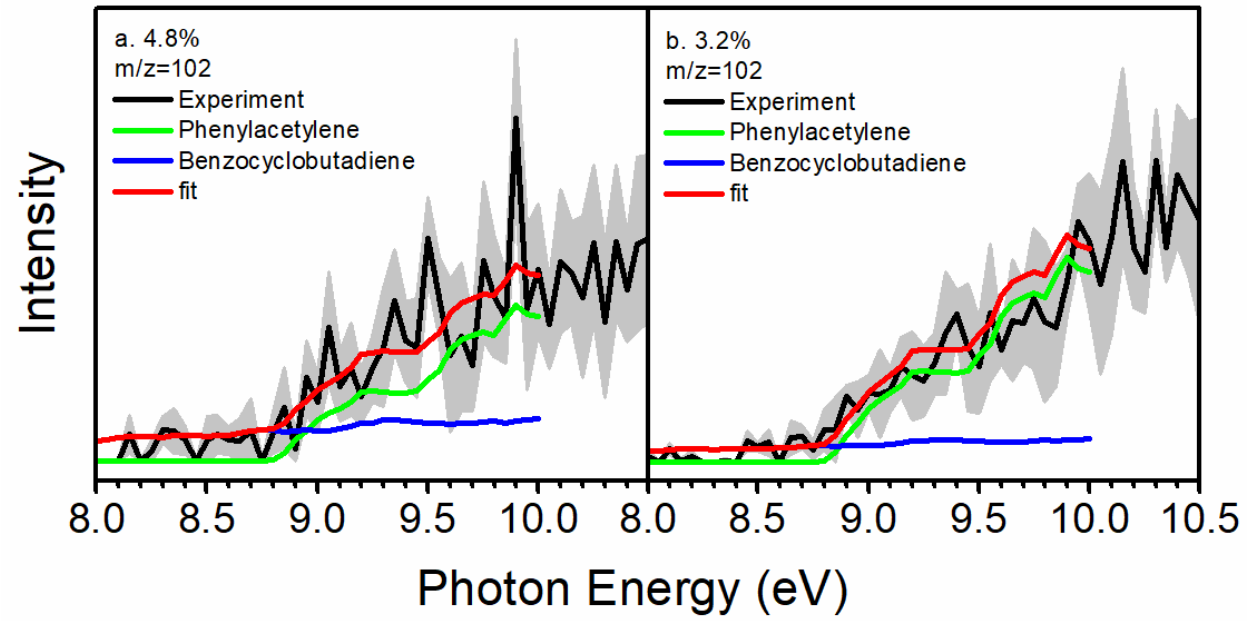

Figure S9. Photoionization efficiency (PIE) curves for signal at *m/z* = 102 in the propargyl recombination system. This signal is only significant at the conditions with the initial mole fractions of propargyl bromide of 4.8% and 3.2%. Black: experimentally derived PIE curves; colored lines (green and blue): reference PIE curves; red lines: overall fit. The percentages exhibited in the figures represent the initial mole fractions of propargyl bromide (C_3H_3Br). As the onset of curve is lower than our experimental measurement range (8.0-10.5 eV), it is unlikely to identify the accurate isomer(s). As benzocyclobutadiene can be produced via the reaction of benzyne and acetylene (*80*), and its adiabatic photoionization energy is 7.5 eV (*81*), it is possible that benzocyclobutadiene contributes to the signal at *m/z* = 102.

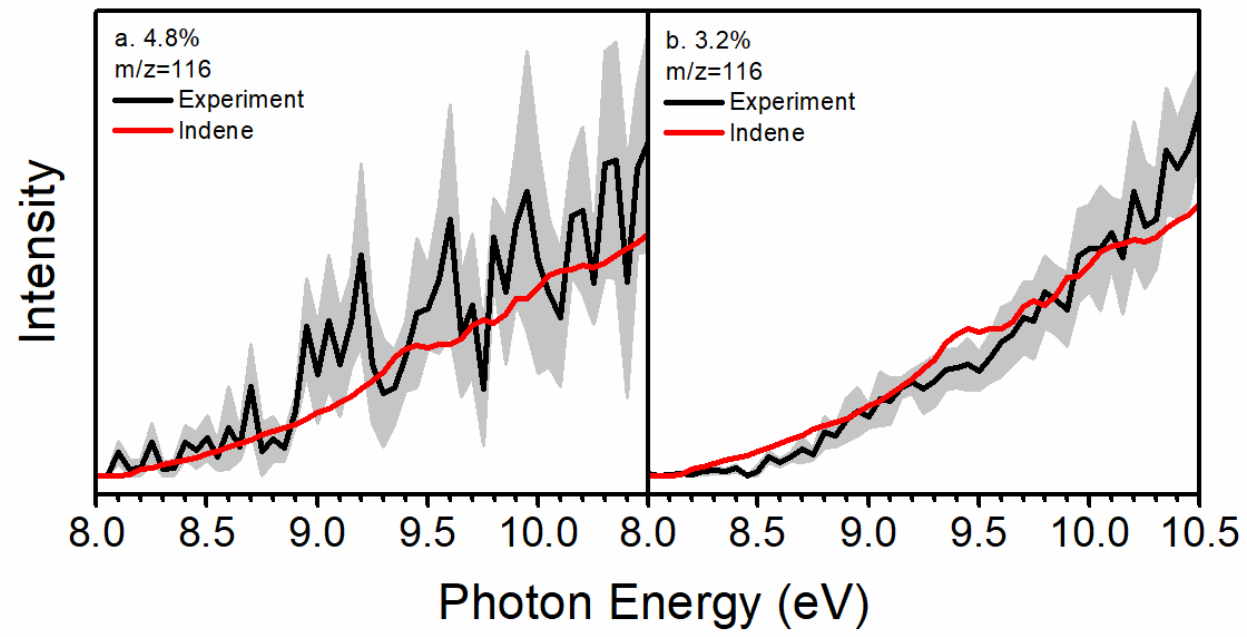

Figure S10. Photoionization efficiency (PIE) curves for signal at *m/z* = 116 in the propargyl recombination system. Black: experimentally derived PIE curves; red lines: reference PIE curve of indene. This signal is only significant at the conditions with the initial mole fractions of propargyl bromide of 4.8% and 3.2%. The percentages exhibited in the figures represent the initial mole fractions of propargyl bromide (C_3H_3Br).

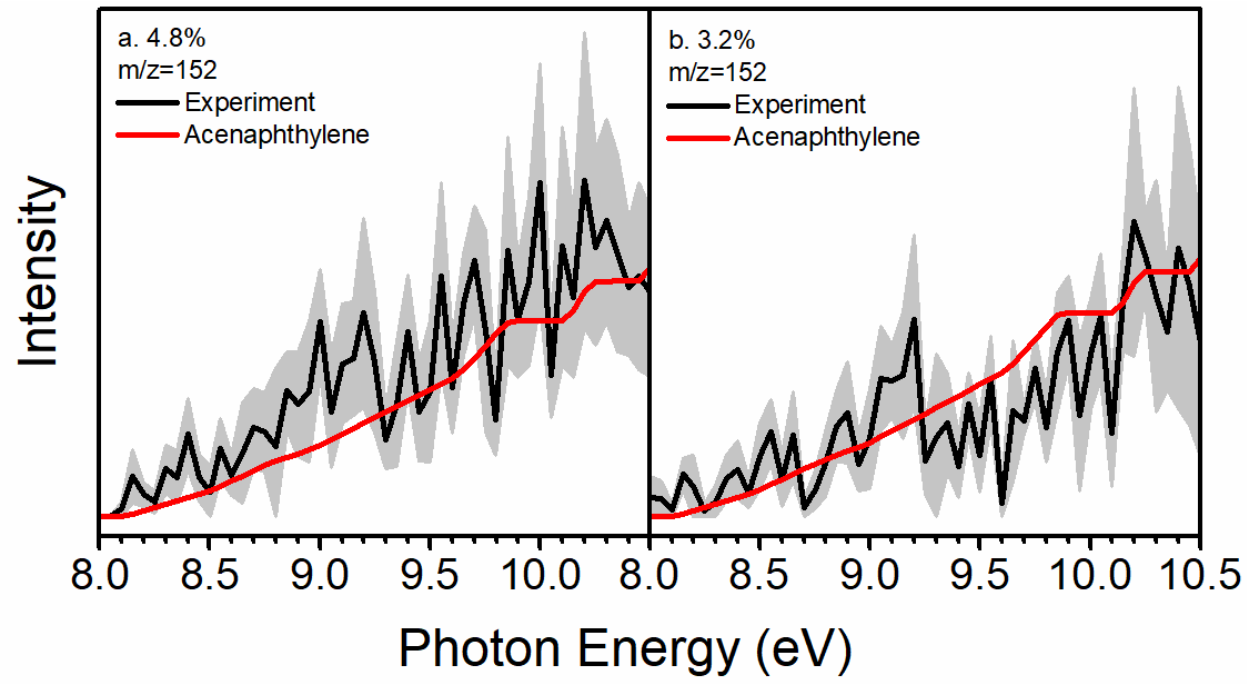

Figure S11. Photoionization efficiency (PIE) curves for signal at *m/z* = 152 in the propargyl recombination system. Black: experimentally derived PIE curves; red lines: reference PIE curve of acenaphthylene. This signal is only significant at the conditions with the initial mole fractions of propargyl bromide of 4.8% and 3.2%. The percentages exhibited in the figures represent the initial mole fractions of propargyl bromide (C_3H_3Br).

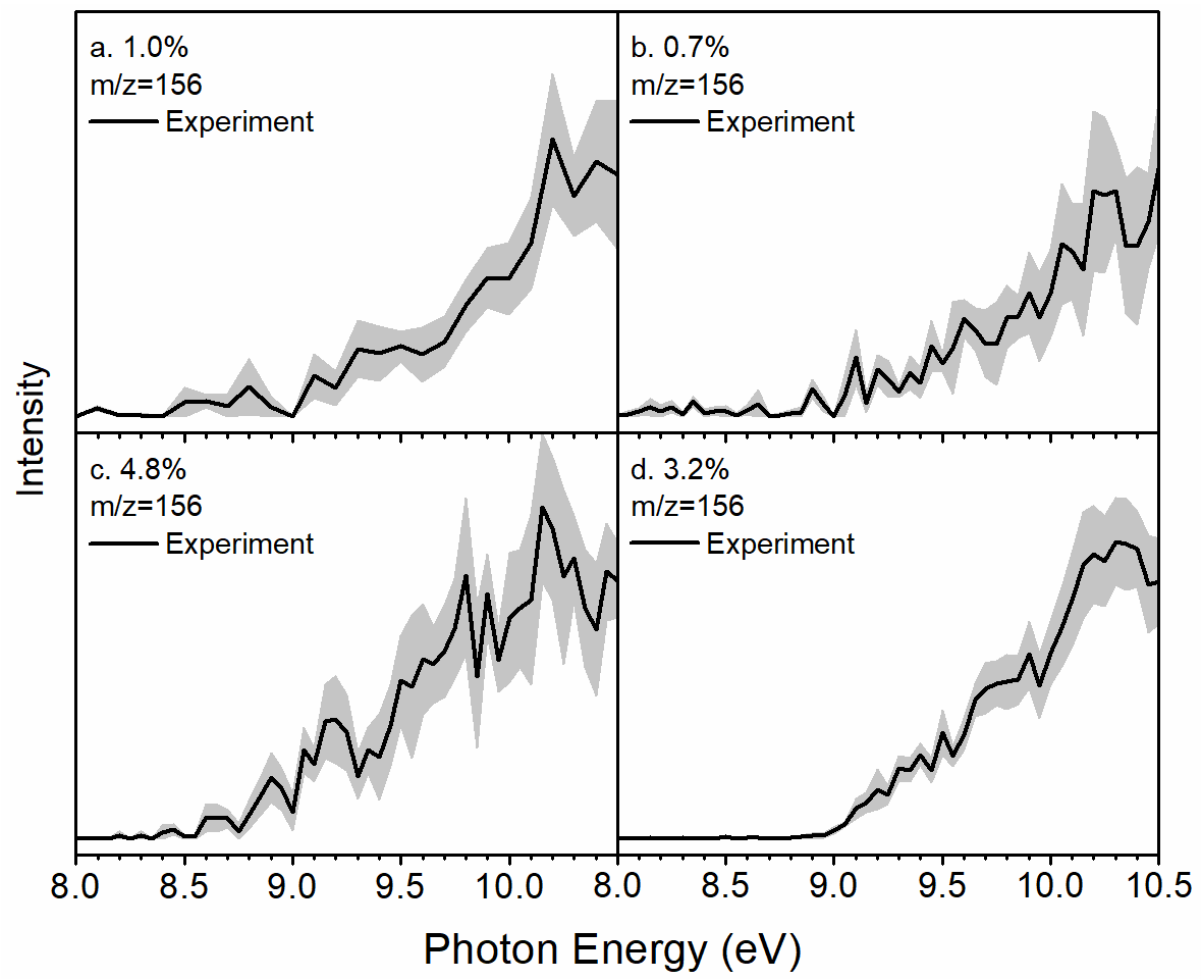

Figure S12. Experimentally derived photoionization efficiency (PIE) curves for signal at *m/z* = 156 in the propargyl recombination system. The percentages exhibited in the figures represent the initial mole fractions of propargyl bromide (C_3H_3Br).

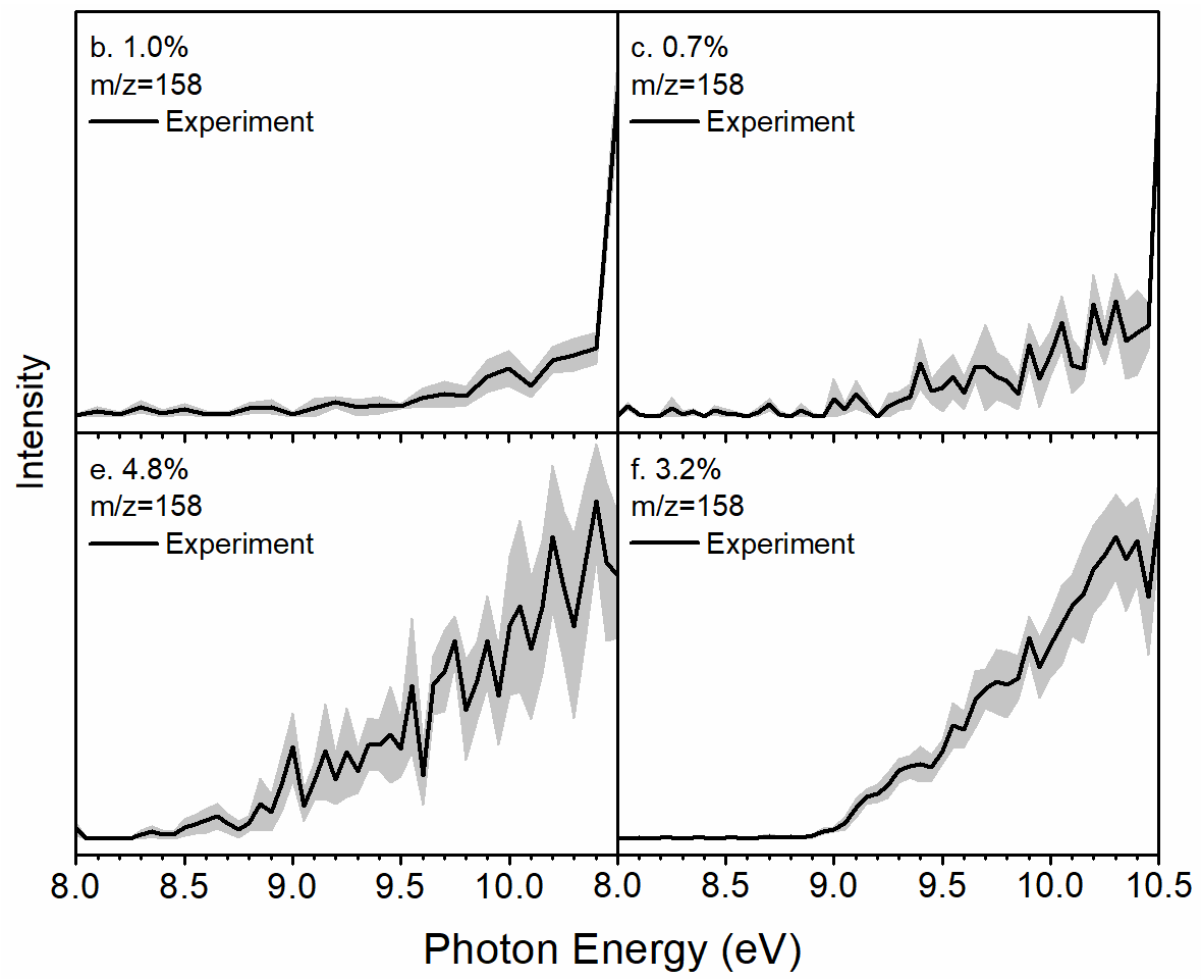

Figure S13. Experimentally derived photoionization efficiency (PIE) curves for signal at *m/z* = 158 in the propargyl recombination system. The percentages exhibited in the figures represent the initial mole fractions of propargyl bromide (C_3H_3Br).

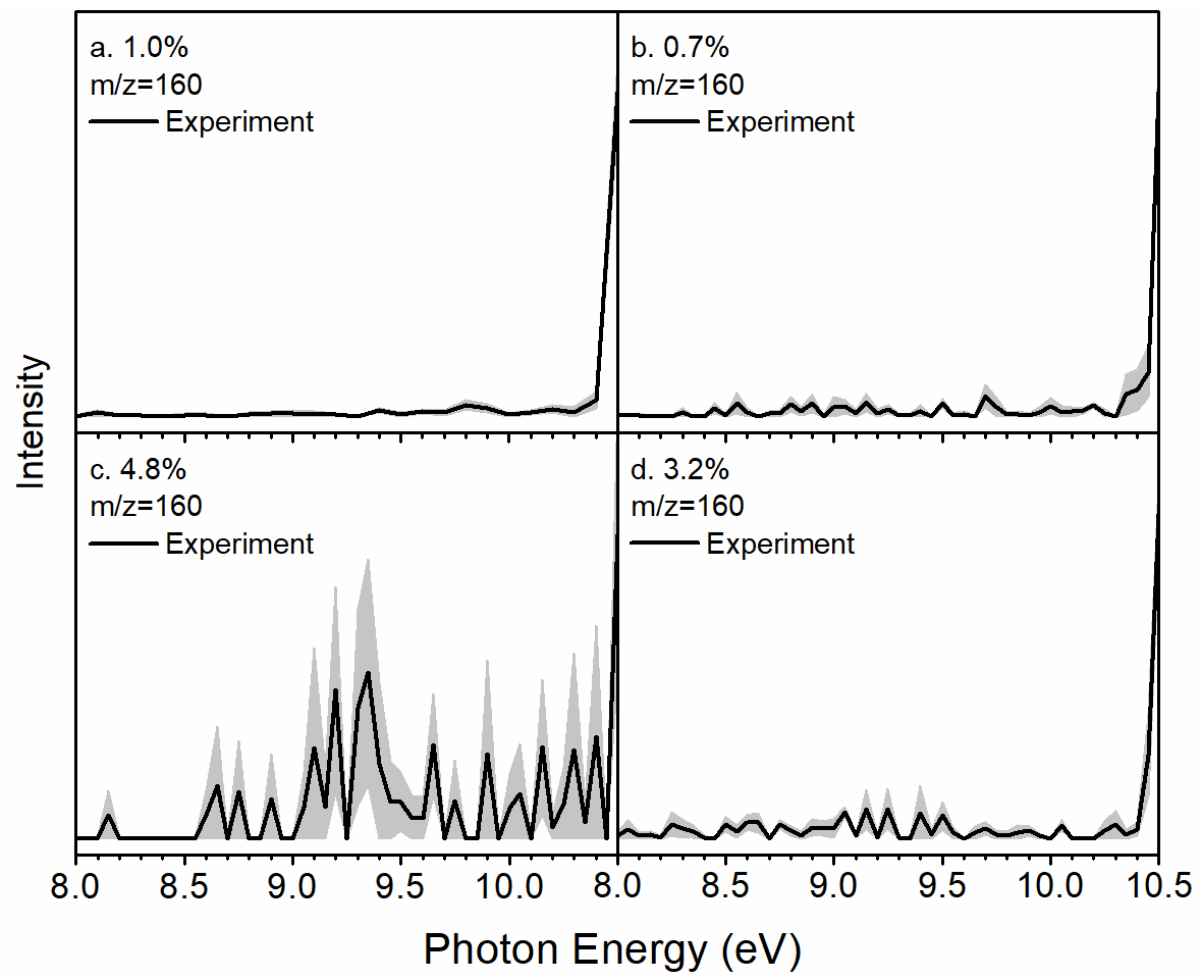

Figure S14. Experimentally derived photoionization efficiency (PIE) curves for signal at *m/z* = 160 in the propargyl recombination system. The percentages exhibited in the figures represent the initial mole fractions of propargyl bromide (C_3H_3Br).

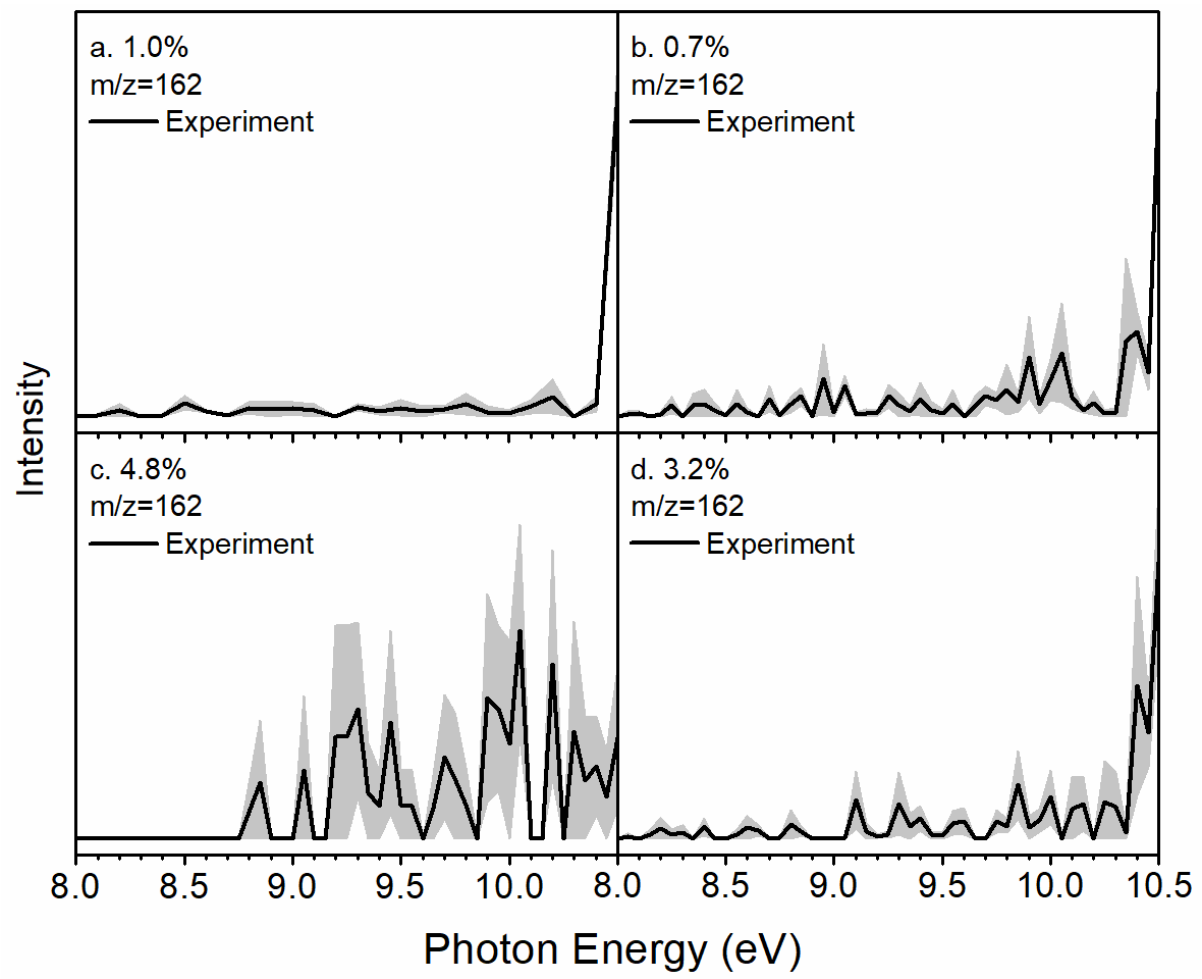

Figure S15. Experimentally derived photoionization efficiency (PIE) curves for signal at *m/z* = 162 in the propargyl recombination system. The percentages exhibited in the figures represent the initial mole fractions of propargyl bromide (C_3H_3Br).

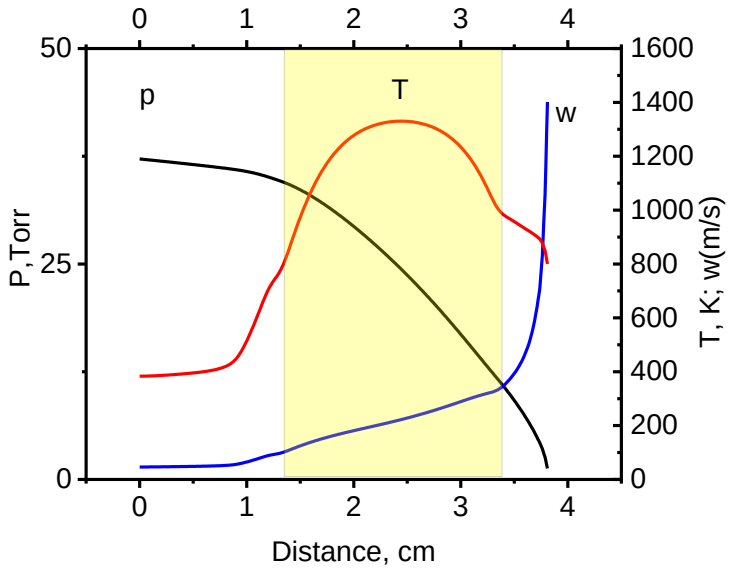

Figure S16. Centerline pressure (left y-axis), temperature and velocity (right y-axis) along the reactor axis. The simulation was performed for the experimental condition with initial mole fraction of propargyl bromide of 1.0%, inlet pressure of 200 torr, reactor temperature at 1343 K. The yellow shaded area defines the electrically heated section of the SiC tube. T: temperature, P: pressure, w: velocity.

REFERENCES AND NOTES

1. A. W. Hofmann, Ueber eine sichere Reaction auf Benzol. *Justus Liebigs Ann. Chem.* **55**, 200–205 (1845).

2. I. Fernandez, Understanding the reactivity of polycyclic aromatic hydrocarbons and related compounds. *Chem. Sci.* **11**, 3769–3779 (2020).

3. P. Sundararajan, M. Tsuge, M. Baba, Y.-P. Lee, Infrared spectrum of protonated corannulene $H^+C_{20}H_{10}$ in solid *para*-hydrogen and its potential contribution to interstellar unidentified infrared bands. *ACS Earth Space Chem.* **2**, 1001–1010 (2018).

4. T. Stein, J. Jose, Molecular formation upon ionization of van der Waals clusters and implication to astrochemistry. *Isr. J. Chem.* **60**, 842–849 (2020).

5. T. B. Mahajan, J. E. Elsila, D. W. Deamer, R. N. Zare, Formation of carbon-carbon bonds in the photochemical alkylation of polycyclic aromatic hydrocarbons. *Orig. Life Evol. Biosph.* **33**, 17–35 (2003).

6. H. Andrews, A. Candian, A. G. G. M. Tielens, Hydrogenation and dehydrogenation of interstellar PAHs: Spectral characteristics and H_2 formation. *Astron. Astrophys.* **595**, A23 (2016).

7. T. I. Mori, I. Sakon, T. Onaka, H. Kaneda, H. Umehata, R. Ohsawa, Diagnosis of PAH properties and ISM conditions based on the near-infrared and mid-infrared UIR bands. *Astron. Soc. Pac. Conf. Ser.* **458**, 133–134 (2012).

8. A. G. G. M. Tielens, The molecular universe. *Rev. Mod. Phys.* **85**, 1021–1081 (2013).

9. A. G. G. M. Tielens, Interstellar polycyclic aromatic hydrocarbon molecules. *Annu. Rev. Astron. Astrophys.* **46**, 289–337 (2008).

10. F. Y. Xiang, A. Li, J. X. Zhong, Diffuse interstellar bands and the ultraviolet extinction curves: The missing link revisited. *Astrophys. J.* **835**, 107 (2017).

11. A. Leger, J. Puget, Identification of the “unidentified IR emission features” of interstellar dust? *Astron. Astrophys.* **137**, L5–L8 (1984).

12. P. Ehrenfreund, M. A. Sephton, Carbon molecules in space: From astrochemistry to astrobiology. *Faraday Discuss.* **133**, 277–288 (2006).

13. E. Herbst, E. F. Van Dishoeck, Complex organic interstellar molecules. *Annu. Rev. Astron. Astrophys.* **47**, 427–480 (2009).

14. J. Puget, A. Léger, A new component of the interstellar matter: Small grains and large aromatic molecules. *Annu. Rev. Astron. Astrophys.* **27**, 161–198 (1989).

15. P. Schmitt-Kopplin, Z. Gabelica, R. D. Gougeon, A. Fekete, B. Kanawati, M. Harir, I. Gebefuegi, G. Eckel, N. Hertkorn, High molecular diversity of extraterrestrial organic matter in Murchison meteorite revealed 40 years after its fall. *Proc. Natl. Acad. Sci. U.S.A.* **107**, 2763–2768 (2010).

16. L. Allamandola, PAHs and astrobiology. *EAS Publ. Ser.* **46**, 305–317 (2011).

17. M. D’Ischia, P. Manini, M. Moracci, R. Saladino, V. Ball, H. Thissen, R. A. Evans, C. Puzzarini, V. Barone, Astrochemistry and astrobiology: Materials science in wonderland? *Int. J. Mol. Sci.* **20**, 4079 (2019).

18. Y. Keheyan, V. Aquilanti, J. R. Brucato, L. Colangeli, F. Cataldo, V. Mennella, Astrochemical and prebiotical elementary processes. *Eur. Space Agency, [Spec. Publ.] SP* **SP-496**, 357–361 (2001).

19. L. M. Ziurys, The chemistry in circumstellar envelopes of evolved stars: Following the origin of the elements to the origin of life. *Proc. Natl. Acad. Sci. U.S.A.* **103**, 12274–12279 (2006).

20. B. O. Prakash, *GSC Biol. Pharm. Sci.* **8**, 081–088 (2019).

21. G. Nagendrappa, Benzene and its isomers. *Resonance* **6**, 74–78 (2001).

22. T. C. Dinadayalane, U. D. Priyakumar, G. N. Sastry, Exploration of C_6H_6 potential energy surface: A computational effort to unravel the relative stabilities and synthetic feasibility of new benzene isomers. *J. Phys. Chem. A* **108**, 11433–11448 (2004).

23. J. A. Miller, C. F. Melius, Kinetic and thermodynamic issues in the formation of aromatic compounds in flames of aliphatic fuels. *Combust. Flame* **91**, 21–39 (1992).

24. C. F. Melius, J. A. Miller, E. M. Evleth, Unimolecular reaction mechanisms involving C_3H_4, C_4H_4, and C_6H_6 hydrocarbon species. *Proc. Combust. Inst.* **24**, 621–628 (1992).

25. L. K. Madden, A. M. Mebel, M. C. Lin, C. F. Melius, Theoretical study of the thermal isomerization of fulvene to benzene. *J. Phys. Org. Chem.* **9**, 801–810 (1996).

26. A. M. Mebel, S. H. Lin, X. M. Yang, Y. T. Lee, Theoretical study on the mechanism of the dissociation of benzene. The $C_5H_3 + CH_3$ product channel. *J. Phys. Chem. A* **101**, 6781–6789 (1997).

27. A. Mebel, M. C. Lin, D. Chakraborty, J. Park, S. H. Lin, Y. T. Lee, Ab initiomolecular orbital/Rice–Ramsperger–Kassel–Marcus theory study of multichannel rate constants for the unimolecular decomposition of benzene and the $H+C_6H_5$ reaction over the ground electronic state. *J. Chem. Phys.* **114**, 8421–8435 (2001).

28. A. M. Mebel, in *Reviews of Modern Quantum Chemistry: A Celebration of the Contributions of Robert G Parr (In 2 Volumes)* (World Scientific, 2002), pp. 340–358.

29. V. Kislov, T. L. Nguyen, A. Mebel, S. Lin, S. Smith, Photodissociation of benzene under collision-free conditions: An ab initio/Rice–Ramsperger–Kassel–Marcus study. *J. Chem. Phys.* **120**, 7008–7017 (2004).

30. J. A. Miller, S. J. Klippenstein, The recombination of propargyl radicals: Solving the master equation. *J. Phys. Chem. A* **105**, 7254–7266 (2001).

31. J. A. Miller, S. J. Klippenstein, The recombination of propargyl radicals and other reactions on a C_6H_6 potential. *J. Phys. Chem. A* **107**, 7783–7799 (2003).

32. E. H. Wilson, S. K. Atreya, A. Coustenis, Mechanisms for the formation of benzene in the atmosphere of Titan. *J. Geophys. Res.* **108**, 8-1–8-10 (2003).

33. B. Sivaraman, R. Mukherjee, K. P. Subramanian, S. B. Banerjee, Benzene formation on interstellar icy mantles containing propargyl alcohol. *Astrophys. J.* **798**, 72 (2015).

34. P. Singh, C.-J. Sung, PAH formation in counterflow non-premixed flames of butane and butanol isomers. *Combust. Flame* **170**, 91–110 (2016).

35. D. L. Baulch, C. J. Cobos, R. A. Cox, P. Frank, G. Hayman, Th. Just, J. A. Kerr, T. Murrells, M. J. Pilling, J. Troe, R. W. Walker, J. Warnatz, Evaluated kinetic data for combustion modeling. supplement I. *J. Phys. Chem. Ref. Data Monogr.* **23**, 847–848 (1994).

36. A. Comandini, T. Malewicki, K. Brezinsky, Chemistry of polycyclic aromatic hydrocarbons formation from phenyl radical pyrolysis and reaction of phenyl and acetylene. *J. Phys. Chem. A* **116**, 2409–2434 (2012).

37. A. Matsugi, A. Miyoshi, Reactions of o-benzyne with propargyl and benzyl radicals: Potential sources of polycyclic aromatic hydrocarbons in combustion. *Phys. Chem. Chem. Phys.* **14**, 9722–9728 (2012).

38. D. S. N. Parker, R. I. Kaiser, B. Bandyopadhyay, O. Kostko, T. P. Troy, M. Ahmed, Unexpected chemistry from the reaction of naphthyl and acetylene at combustion-like temperatures. *Angew. Chem. Int. Ed. Engl.* **54**, 5421–5424 (2015).

39. T. Yang, R. I. Kaiser, T. P. Troy, B. Xu, O. Kostko, M. Ahmed, A. M. Mebel, M. V. Zagidullin, V. N. Azyazov, HACA's heritage: A free-radical pathway to phenanthrene in circumstellar envelopes of asymptotic giant branch stars, *Angew. Chem. Int. Ed. Engl.* **56**, 4515–4519 (2017).

40. L. Zhao, R. I. Kaiser, B. Xu, U. Ablikim, M. Ahmed, M. M. Evseev, E. K. Bashkirov, V. N. Azyazov, A. M. Mebel, Low-temperature formation of polycyclic aromatic hydrocarbons in Titan's atmosphere. *Nat. Astron.* **2**, 973–979 (2018).

41. G. Bieri, F. Burger, E. Heilbronner, J. P. Maier, Valence ionization energies of hydrocarbons. *Helv. Chim. Acta* **60**, 2213–2233 (1977).

42. R. I. Kaiser, Experimental investigation on the formation of carbon-bearing molecules in the interstellar medium via neutral−neutral reactions. *Chem. Rev.* **102**, 1309–1358 (2002).

43. S. Soorkia, A. J. Trevitt, T. M. Selby, D. L. Osborn, C. A. Taatjes, K. R. Wilson, S. R. Leone, Reaction of the C_2H radical with 1-butyne (C_4H_6): Low-temperature kinetics and isomer-specific product detection. *J. Phys. Chem. A* **114**, 3340–3354 (2010).

44. T. A. Cool, J. Wang, K. Nakajima, C. A. Taatjes, A. Mcllroy, Photoionization cross sections for reaction intermediates in hydrocarbon combustion. *Int. J. Mass Spectrom.* **247**, 18–27 (2005).

45. H. M. Rosenstock, K. E. McCulloh, F. P. Lossing, On the mechanisms of C_6H_6 ionization and fragmentation. *Int. J. Mass Spectrom. Ion Phys.* **25**, 327–341 (1977).

46. Y. Li, J. Yang, Z. Cheng, *Photonionization Cross Section Database (Version 2.0)* (National Synchrotron Radiation Laboratory, Hefei, China, 2017); http://flame.nsrl.ustc.edu.cn/database/.

47. N. Hansen, J. A. Miller, C. A. Taatjes, J. Wang, T. A. Cool, M. E. Law, P. R. Westmoreland, Photoionization mass spectrometric studies and modeling of fuel-rich allene and propyne flames. *Proc. Combust. Inst.* **31**, 1157–1164 (2007).

48. J. D. Savee, S. Soorkia, O. Welz, T. M. Selby, C. A. Taatjes, D. L. Osborn, Absolute photoionization cross-section of the propargyl radical. *J. Chem. Phys.* **136**, 134307 (2012).

49. L. Zhao, R. I. Kaiser, B. Xu, U. Ablikim, M. Ahmed, M. V. Zagidullin, V. N. Azyazov, A. H. Howlader, S. F. Wnuk, A. M. Mebel, VUV photoionization study of the formation of the simplest polycyclic aromatic hydrocarbon: Naphthalene (C10H8). *J. Phys. Chem. Lett.* **9**, 2620–2626 (2018).

50. M. Zagidullin, R. I. Kaiser, D. P. Porfiriev, I. P. Zavershinskiy, M. Ahmed, V. N. Azyazov, A. M. Mebel, Functional relationships between kinetic, flow, and geometrical parameters in a high-temperature chemical microreactor. *J. Phys. Chem. A* **122**, 8819–8827 (2018).

51. L. Zhao, R. I. Kaiser, B. Xu, U. Ablikim, W. Lu, M. Ahmed, M. M. Evseev, E. K. Bashkirov, V. N. Azyazov, M. V. Zagidullin, Gas phase synthesis of [4]-helicene. *Nat. Commun.* **10**, 1510 (2019).

52. D. S. N. Parker, F. Zhang, Y. S. Kim, R. I. Kaiser, A. Landera, V. V. Kislov, A. M. Mebel, A. G. G. M. Tielens, Low temperature formation of naphthalene and its role in the synthesis of PAHs (Polycyclic Aromatic Hydrocarbons) in the interstellar medium. *Proc. Natl. Acad. Sci. U.S.A.* **109**, 53–58 (2012).

53. R. I. Kaiser, D. S. N. Parker, A. M. Mebel, *Annual Review of Physical Chemistry, Vol 66*, M. A. Johnson, T. J. Martinez, Eds. (Annual Reviews, 2015), vol. 66, pp. 43–67.

54. B. M. Jones, F. Zhang, R. I. Kaiser, A. Jamal, A. M. Mebel, M. A. Cordiner, S. B. Charnley, Formation of benzene in the interstellar medium. *Proc. Natl. Acad. Sci. U.S.A.* **108**, 452–457 (2011).

55. N. Balucani, O. Asvany, A. H. H. Chang, S. H. Lin, Y. T. Lee, R. I. Kaiser, H. F. Bettinger, P. . R. Schleyer, H. F. Schaefer III, Crossed beam reaction of cyano radicals with hydrocarbon molecules. I. Chemical dynamics of cyanobenzene (C_6H_5CN; X^1A_1) and perdeutero cyanobenzene (C_6D_5CN; X^1A_1) formation from reaction of $CN(X^2\Sigma^+)$ with benzene C6H6(X^1A_{1g}), and d_6-benzene $C_6D_6(X^1A_{1g})$. *J. Chem. Phys.* **111**, 7457–7471 (1999),.

56. B. A. McGuire, A. M. Burkhardt, S. Kalenskii, C. N. Shingledecker, A. J. Remijan, E. Herbst, M. C. McCarthy, Detection of the aromatic molecule benzonitrile (c-C_6H_5CN) in the interstellar medium. *Science* **359**, 202–205 (2018).

57. J. C. Loison, M. Dobrijevic, K. M. Hickson, The photochemical production of aromatics in the atmosphere of Titan. *Icarus* **329**, 55–71 (2019).

58. M. López-Puertas, B. M. Dinelli, A. Adriani, B. Funke, M. García-Comas, M. L. Moriconi, E. D'Aversa, C. Boersma, L. J. Allamandola, Large abundances of polycyclic aromatic hydrocarbons in Titan's upper atmosphere. *Astrophys. J.* **770**, 132 (2013).

59. N. Hansen, X. He, R. Griggs, K. Moshammer, Knowledge generation through data research: New validation targets for the refinement of kinetic mechanisms. *Proc. Combust. Inst.* **37**, 743–750 (2019).

60. F. T. Zhang, R. I. Kaiser, V. V. Kislov, A. M. Mebel, A. Golan, M. Ahmed, A VUV photoionization study of the formation of the indene molecule and its isomers. *J. Phys. Chem. Lett.* **2**, 1731–1735 (2011).

61. F. Qi, Combustion chemistry probed by synchrotron VUV photoionization mass spectrometry. *Proc. Combust. Inst.* **34**, 33–63 (2013).

62. K. N. Urness, Q. Guan, A. Golan, J. W. Daily, M. R. Nimlos, J. F. Stanton, M. Ahmed, G. B. Ellison, Pyrolysis of furan in a microreactor. *J. Chem. Phys.* **139**, 124305 (2013).

63. Y. Georgievskii, J. A. Miller, S. J. Klippenstein, Association rate constants for reactions between resonance-stabilized radicals: $C_3H_3 + C_3H_3$, $C_3H_3 + C_3H_5$, and $C_3H_5 + C_3H_5$. *Phys. Chem. Chem. Phys.* **9**, 4259–4268 (2007).

64. L. B. Harding, Y. Georgievskii, S. J. Klippenstein, Predictive theory for hydrogen atom−hydrocarbon radical association kinetics. *J. Phys. Chem. A* **109**, 4646–4656 (2005).

65. Y. Georgievskii, S. J. Klippenstein, Variable reaction coordinate transition state theory: Analytic results and application to the $C_2H_3+H \rightarrow C_2H_4$ reaction. *J. Chem. Phys.* **118**, 5442–5455 (2003).

66. Y. Georgievskii, S. J. Klippenstein, Transition state theory for multichannel addition reactions: Multifaceted dividing surfaces. *J. Phys. Chem. A* **107**, 9776–9781 (2003).

67. C. L. Morter, S. K. Farhat, J. D. Adamson, G. P. Glass, R. F. Curl, Rate constant measurement of the recombination reaction $C_3H_3 + C_3H_3$. *J. Phys. Chem* **98**, 7029–7035 (1994).

68. D. B. Atkinson, J. W. Hudgens, Rate coefficients for the propargyl radical self-reaction and oxygen addition reaction measured using ultraviolet cavity ring-down spectroscopy. *J. Phys. Chem. A* **103**, 4242–4252 (1999).

69. A. Fahr, A. Nayak, Kinetics and products of propargyl (C_3H_3) radical self-reactions and propargyl-methyl cross-combination reactions. *Int. J. Chem. Kinet.* **32**, 118–124 (2000).

70. P.-T. Howe, A. Fahr, Pressure and temperature effects on product channels of the propargyl ($HC{:}CCH_2$) combination reaction and the formation of the “First Ring”. *J. Phys. Chem. A* **107**, 9603–9610 (2003).

71. S. Scherer, T. Just, P. Frank, High-temeprature investigations on pyrolytic reactions of propargyl radicals. *Proc. Combust. Inst.* **28**, 1511–1518 (2000).

72. J. D. DeSain, C. A. Taatjes, Infrared laser absorption measurements of the kinetics of propargyl radical self-reaction and the 193 nm photolysis of propyne. *J. Phys. Chem. A* **107**, 4843–4850 (2003).

73. E. V. Shafir, I. R. Slagle, V. D. Knyazev, Kinetics and products of the self-reaction of propargyl radicals. *J. Phys. Chem. A* **107**, 8893–8903 (2003).

74. B. Giri, H. Hippler, M. Olzmann, A. Unterreiner, The rate coefficient of the $C_3H_3 + C_3H_3$ reaction from UV absorption measurements after photolysis of dipropargyl oxalate. *Phys. Chem. Chem. Phys.* **5**, 4641–4646 (2003).

75. R. Fernandes, H. Hippler, M. Olzmann, Determination of the rate coefficient for the $C_3H_3 + C_3H_3$ reaction at high temperatures by shock-tube investigations. *Proc. Combust. Inst.* **30**, 1033–1038 (2005).

76. C. L. Rasmussen, M. S. Skjøth-Rasmussen, A. D. Jensen, P. Glarborg, Propargyl recombination: Estimation of the high temperature, low pressure rate constant from flame measurements. *Proc. Combust. Inst.* **30**, 1023–1031 (2005).

77. W. Tang, R. S. Tranter, K. Brezinsky, Isomeric product distributions from the self-reaction of propargyl radicals. *J. Phys. Chem. A* **109**, 6056–6065 (2005).

78. D. L. Osborn, C. A. Taatjes, F. Goulay, T. M. Selby, P. Zou, A. Fahr, *A Time-Resolved Isomer-Resolved Study of the Propargyl Self Reaction Using a Multiplexed Photoionization Mass Spectrometer* (Sandia National Lab, 2010).

79. P. Constantinidis, F. Hirsch, I. Fischer, A. Dey, A. M. Rijs, Products of the propargyl self-reaction at high temperatures investigated by IR/UV Ion dip spectroscopy. *J. Phys. Chem. A* **121**, 181–191 (2017).

80. G. Friedrichs, E. Goos, J. Gripp, H. Nicken, J.-B. Schönborn, H. Vogel, F. Temps, The products of the reactions of *o*-benzyne with ethene, propene, and acetylene: A combined mass spectrometric and quantum chemical study. *Z. Phys. Chem.* **223**, 387–407 (2009).

81. T. Koenig, D. Imre, J. A. Hoobler, Helium (He I) photoelectron spectrum of benzocyclobutadiene. *J. Am. Chem. Soc.* **101**, 6446–6447 (1979).

82. D. S. Parker, R. I. Kaiser, T. P. Troy, M. Ahmed, Hydrogen abstraction/acetylene addition revealed. *Angew. Chem. Int. Edit.* **53**, 7740–7744 (2014).

83. J. Z. Yang, L. Zhao, J. H. Cai, F. Qi, Y. Y. Li, Photoionization mass spectrometric and kinetic modeling of low-pressure Pyrolysis of Benzene. *Chin. J. Chem. Phys.* **26**, 245–251 (2013).

84. S. L. Peukert, N. J. Labbe, R. Sivaramakrishnan, J. V. Michael, Direct measurements of rate constants for the reactions of CH_3 radicals with C_2H_6, C_2H_4, and C_2H_2 at high temperatures. *J. Phys. Chem. A* **117**, 10228–10238 (2013).

85. S. Fujisawa, K. Ohno, S. Masuda, Y. Harada, Penning ionization electron spectroscopy of monohalobenzenes: Fluorobenzene, chlorobenzene, bromobenzene, and iodohenzene. *J. Am. Chem. Soc.* **108**, 6505–6511 (1986).

86. A. Yencha, A. Hopkirk, A. Hiraya, R. J. Donovan, J. G. Goode, R. R. J. Maier, G. C. King, A. Kvaran, Threshold photoelectron spectroscopy of Cl_2 and Br_2 up to 35 eV. *J. Phys. Chem.* **99**, 7231–7241 (1995).

87. Q. Guan, K. N. Urness, T. K. Ormond, D. E. David, G. Barney Ellison, J. W. Daily, The properties of a micro-reactor for the study of the unimolecular decomposition of large molecules. *Int. Rev. Phys. Chem.* **33**, 447–487 (2014).

88. Comsol Multiphysics, *Version 4.3b* (Comsol, Inc., Los Angeles, CA, USA, 2007); http://www.comsol.com.

89. B. Yang, J. Wang, T. A. Cool, N. Hansen, S. Skeen, D. L. Osborn, Absolute photoionization cross-sections of some combustion intermediates. *Int. J. Mass spectrom.* **309**, 118–128 (2012).

90. T. A. Cool, K. Nakajima, C. A. Taatjes, A. McIlroy, P. R. Westmoreland, M. E. Law, A. Morel, Studies of a fuel-rich propane flame with photoionization mass spectrometry. *Proc. Combust. Inst.* **30**, 1681–1688 (2005).

91. J. A. Miller, S. J. Klippenstein, From the multiple-well master equation to phenomenological rate coefficients: Reactions on a C_3H_4 potential energy surface. *J. Phys. Chem. A* **107**, 2680–2692 (2003).

92. Y. Hidaka, T. Nakamura, A. Miyauchi, T. Shiraishi, H. Kawano, Thermal decomposition of propyne and allene in shock waves. *Int. J. Chem. Kinet.* **21**, 643–666 (1989).

93. A. S. Semenikhin, A. S. Savchenkova, I. V. Chechet, S. G. Matveev, Z. Liu, M. Frenklach, A. M. Mebel, Rate constants for H abstraction from benzo(a)pyrene and chrysene: A theoretical study. *Phys. Chem. Chem. Phys.* **19**, 25401–25413 (2017).

94. A. W. Jasper, N. Hansen, Hydrogen-assisted isomerizations of fulvene to benzene and of larger cyclic aromatic hydrocarbons. *Proc. Combust. Inst.* **34**, 279–287 (2013).

95. L. V. Moskaleva, L. K. Madden, M. C. Lin, Unimolecular isomerization/decomposition of ortho-benzyne: Ab initio MO/statistical theory study. *Phys. Chem. Chem. Phys.* **1**, 3967–3972 (1999).

96. V. V. Kislov, N. I. Islamova, A. M. Kolker, S. H. Lin, A. M. Mebel, Hydrogen abstraction acetylene addition and Diels–Alder mechanisms of PAH formation: A detailed study using first principles calculations. *J. Chem. Theory Comput.* **1**, 908–924 (2005).

97. R. S. Tranter, S. J. Klippenstein, L. B. Harding, B. R. Giri, X. Yang, J. H. Kiefer, Experimental and theoretical investigation of the self-reaction of phenyl radicals. *J. Phys. Chem. A* **114**, 8240–8261 (2010).

98. A. N. Morozov, A. M. Mebel, Theoretical study of the reaction mechanism and kinetics of the phenyl + propargyl association. *Phys. Chem. Chem. Phys.* **22**, 6868–6880 (2020).

99. T. Zhang, X. N. Tang, K. C. Lau, C. Y. Ng, C. Nicolas, D. S. Peterka, M. Ahmed, M. L. Morton, B. Ruscic, R. Yang, L. X. Wei, C. Q. Huang, B. Yang, J. Wang, L. S. Sheng, Y. W. Zhang, F. Qi, Direct identification of propargyl radical in combustion flames by vacuum ultraviolet photoionization mass spectrometry. *J. Chem. Phys.* **124**, 074302 (2006).